



This project has received funding from the European Union's Horizon 2020 research and innovation programme under grant agreement No 101016608.

BEYOND 5G – OPTICAL NETWORK CONTINUUM
(H2020 – Grant Agreement N° 101016663)

Deliverable D3.2

Second year results on data plane infrastructure

Editor N. Calabretta (TUE)

Contributors TIM, BT, ADVA, NOKIA, CNIT, CTTC, INF-P, INF-D, HHI, OLC-E, TUE, PLF

Version 2.5

Date November 13, 2023

Distribution PUBLIC (PU)



DISCLAIMER

This document contains information, which is proprietary to the B5G-OPEN (Beyond 5G – Optical nEtnetwork coNtinuum) consortium members that is subject to the rights and obligations and to the terms and conditions applicable to the Grant Agreement number 101016663. The action of the B5G-OPEN consortium members is funded by the European Commission.

Neither this document nor the information contained herein shall be used, copied, duplicated, reproduced, modified, or communicated by any means to any third party, in whole or in parts, except with prior written consent of the B5G-OPEN consortium members. In such case, an acknowledgement of the authors of the document and all applicable portions of the copyright notice must be clearly referenced. In the event of infringement, the consortium members reserve the right to take any legal action it deems appropriate.

This document reflects only the authors' view and does not necessarily reflect the view of the European Commission. Neither the B5G-OPEN consortium members as a whole, nor a certain B5G-OPEN consortium member warrant that the information contained in this document is suitable for use, nor that the use of the information is accurate or free from risk, and accepts no liability for loss or damage suffered by any person using this information.

The information in this document is provided as is and no guarantee or warranty is given that the information is fit for any particular purpose. The user thereof uses the information at its sole risk and liability.

REVISION HISTORY

Revision	Date	Responsible	Comment
1.0	<i>September 4, 2023</i>	<i>N. Calabretta</i>	<i>First draft</i>
2.0	<i>October 27, 2023</i>	<i>N. Calabretta</i>	
2.1	<i>October 31, 2023</i>	<i>N. Calabretta</i>	
2.2	<i>November 2, 2023</i>	<i>N. Calabretta</i>	
2.3	<i>November 10, 2023</i>	<i>E. Riccardi</i>	<i>Document revision</i>
2.4	<i>November 10, 2023</i>	<i>Albert Rafel</i>	<i>Document revision</i>
2.5	<i>November 13, 2023</i>	<i>N. Calabretta</i>	<i>Final version</i>

LIST OF AUTHORS

<i>Partner ACRONYM</i>	<i>Partner FULL NAME</i>	<i>Name & Surname</i>
TUE	<i>Technische Universiteit Eindhoven</i>	<i>Nicola Calabretta, Shiyi Xia</i>
TIM	<i>Telecom Italia SPA</i>	<i>Anna Chiado' Piat, Marco Quagliotti, Emilio Riccardi</i>
BT	<i>British Telecommunications Public Limited Company</i>	<i>Albert Rafel</i>
INF-G	<i>Coriant R&D GmbH</i>	<i>Antonio Napoli, Carlos Castro</i>
INF-P	<i>Infinera Unipessoal, Lda</i>	<i>Nelson Costa, João Pedro</i>
ADVA	<i>ADVA SE</i>	<i>Lutz Rapp</i>
CNIT	<i>Consorzio Nazionale Interuniversitario Per Le Telecomunicazioni</i>	<i>Filippo Cugini, Francesco Paolucci</i>
CTTC	<i>Centre Tecnològic de Telecomunicacions de Catalunya</i>	<i>Laia Nadal, Ramon Casellas, Ricardo Martínez, Francisco Javier Vilchez and Michela Svaluto Moreolo</i>
HHI	<i>Fraunhofer Gesellschaft</i>	<i>Caio Santos, Behnam Shariati, Johannes K. Fischer</i>
OLC-E	<i>OpenLightComm Europe</i>	<i>Alexandros Stavdas, Christos Matrakidis, Dimitris Uzunidis</i>
Nokia	<i>Nokia Network France</i>	<i>Fabien Boitier, Patricia Layec, Alix May, Petros Ramantanis</i>
PLF	<i>pureLiFi Limited</i>	<i>Rui Bian</i>

GLOSSARY

Acronym	Expansion
5G	Fifth Generation
ADM	Add/Drop Multiplexer
AP	Access Point
APD	Avalanche photodiode
API	Application Programming Interface
ASE	Amplifier Spontaneous Emission
B2B	Back to back
B5G	Beyond 5G
BER	Bit Error Ratio
BFD	Bidirectional Forwarding Detection
BPF	Band pass filter
BPSK	Binary Phase-shift keying
BVT	Bandwidth/bit rate Variable Transceivers
CAGR	Compound Annual Growth Rate
Capex	Capital Expenditure
CD	Chromatic dispersion
CNF	Cloud-native Network Function
CO	Central Office
CP	Cyclic Prefix
CPRI	Common Public Radio Interface
C-RAN	Centralized-Radio Access Network
CUT	Channels under test
DAC	Digital Analog Convertor
DC	Data Center
DSC	Digital Subcarrier
DSCM	Digital Subcarrier Multiplexing
DSP	Digital Signal Processing
DU	Distributed Unit
DWDM	Dense Wavelength Division Multiplexing
E/O	Electrical to Optical

EC	European Commission
ECOC	European Conference on Optical Communications
eCPRI	Enhanced CPRI
EDFA	Erbium Doped Fiber Amplifier
Eth.	Ethernet
ETSI	European Telecommunication Standards Institute
ETSI MANO	ETSI NFV Management and. Orchestration
FEC	Forward error correction
FFT	Fast Fourier transform
FWM	Four-Wave Mixing
GN	Gaussian Noise
GSNR	Generalized Signal-to-Noise Ratio
HD	Hard Decision
HFA	Hybrid erbium-doped fiber (EDF)/Raman amplifiers
IFFT	inverse fast Fourier transform
INT	In-band Network Telemetry
IoT	Internet-of-Things
IP	Internet Protocol
ISRS	Inter-channel Stimulated Raman Scattering
ITU	International Telecommunication Union
KPI	Key Performance Indicator
LED	Light-emitting diode
LiFi	Light Fidelity
LLS	Low Layer Split
MAC	Media Access Control
MAN	Metropolitan Area Network
MAS	Multi-Agent System
MB	Multi-Band
MBH	Mobile Back-Haul
MBN	Multi-Band Network
MCF	Multi-Core Fiber
MCM	Multicarrier modulation
MCS	Multi-Cast Switch
MFH	Mobile Front-Haul

MIMO	Multiple-Input Multiple-Output
ML	Machine Learning
MLNT	Multi-Layer Network Telemetry
MMH	Mobile Mid-Haul
MMI	Multi-Mode Interference
mMIMO	Massive MIMO
NCC	Network and Computing Convergence
NF	Noise Figure
NFV	Network Function Virtualization
NG	Next Generation
NGC	Next Generation Core
NMS	Network Management System
NOS	Node Operating System
NR	New Radio
O/E/O	Optical to Electrical to Optical
OADM	Optical Add/Drop Multiplexer
OD	Origin-Destination
ODN	Optical Distribution Network
OFC	Optical Networking and Communication Conference & Exhibition
OFDM	Orthogonal Frequency Division Multiplexing
OFDM	Orthogonal Frequency Division Multiplexing.
OIF-ENMI	OIF External Network to Network Interface
OLA	Optical Line Amplifier
OLS	Open Line system
OLT	Optical Line Terminal
ONF	Open Networking Foundation
ONT	Optical Network Termination
ONU	Optical Network Unit
Opex	Operational Expenditure
OSC	Oscilloscope
OSNIR	Optical Signal-To-Noise plus Interference Ratio
OSNR	Optical Signal-To-Noise Ratio
OSS	Operation Support Systems

OTDR	Optical Time Domain Reflectometer
OTN	Optical Transport Network
OTT	Over-The-Top
OXC	Optical Cross-Connect
P2MP	Point-To-MultiPoint
PCE	Path Computational Engine
PCEP	Path Computation Element Communication Protocol
PDL	Polarization-dependent loss
PDLA	Polarization-dependent loss analyzer
PDM	Polarization-division multiplexed
PE	P-Edge
PHY	Physical layer
PIC	Photonic integrated circuit
PM	Project Manager
PMD	Physical Medium Dependent
PO	Project Officer
PoC	Proof of Concept
PON	Passive Optical Network
POP	Point Of Presence
PPDU	Physical layer protocol data unit
PPP	Point-to-Point Protocol
PtMP	Point-to-Multi-Point
PtoP	Point-to-Point
QAM	Quadrature amplitude modulation
QMR	Quarterly Management Reports
QoE	Quality of Experience
QoS	Quality of Service
QoT	Quality of Transmission
QPSK	Quadrature Phase Shift Keying
QSFP	Quad Small Form-factor Pluggable
R&D	Research and Development
RAN	Radio Access Network
RAT	Radio Access Technology
RL	Reinforcement Learning

RMSA	Routing, Modulation and Spectrum Assignment
RMSE	Root mean square error
ROADM	Reconfigurable Optical Add/Drop Multiplexer
RoF	Radio Over Fiber
RRH	Remote Radio Head
RRU	Remote Radio Unit
RTT	Round-Trip Time
RU	Radio Unit
S-BVT	Sliceable Bandwidth/bitrate Variable Transceiver
SC	Steering Committee
SDM	Space Division Multiplexing
SDN	Software Defined Networking
SDO	Standards Developing Organization
SD-WAN	Software Defined WAN
SL	Supervised Learning
SLA	Service Level Agreement
SME	Small and Medium-sized Enterprises
SoA	State of the Art
SOA	Semiconductor optical Amplifier
SONiC	Software for Open Networking in the Cloud
SRS	Stimulated Raman Scattering
SSB	Single side band
SSF	Split Step Fourier
SSMF	Single mode fibre
STIN	Space-Terrestrial Integrated Network
TC	Technical Committee
TCO	Total Cost of Ownership
TDFA	Thulium-Doped Fiber Amplifier
TDM	Time Division Multiplexing
TIP	Telecom Infra Project
TIRO	Tactile Internet and Remote Operations
TLS	Tunable Laser Source
TM	Technical Manager
TRL	Technology Readiness Levels



UE	User Equipment
UNI	User Network Interface
UP	User Plane
uRLLC	Ultra-Reliable Low Latency Communication
VLAN	Virtual Local Area Network

EXECUTIVE SUMMARY

This deliverable reports on the activities of WP3 during the second year of the project. The work was split into different activities with the following objectives:

1. Design of an innovative optical transport infrastructure supporting MB connectivity and transparent network continuum potentially from User Equipment to Data Centers.
2. Modelling transmission and traffic performance of the identified MB data plane solutions.
3. Design, prototyping and experimental assessment of the novel optical network devices for switching, amplification and transmission.
4. Exploring and testing optical innovative solutions for MB PON, Point to Multi-point (PtMP) with low cost and power consumption for next-generation optical access & 5G X-haul.
5. Design and testing the effective integration of fiber with LiFi systems supporting multi-cell simultaneous transmission for bandwidth maximization and effective hand-over.
6. Design, prototyping and testing advanced monitoring solutions to enable efficient and flexible use of the infrastructure.

To achieve the second objective, this document utilizes the reference architecture discussed in D3.1. It provides an overall view of the architecture and design standards for optical nodes and transmission systems in different network segments (backbone, metropolitan core, and metropolitan aggregation). The updates here primarily consider three reference time frame scenarios: short-term, mid-term, and long-term (approximately 3 years, 6 years, and 9 years from now, respectively). For each scenario, estimated traffic demands in various networks are provided using the traffic model developed in D2.1.. This analysis serves as the foundation for guiding the introduction of new technologies and architectures in different network segments and time frame scenarios.

In the metropolitan core networks, it is suggested that, starting from the short-term scenario, C+L band systems or SDM (Space Division Multiplexing) may be deployed. In the metropolitan aggregation section, the currently deployed C-band is expected to suffice for meeting the requirements of the mid-term scenario (utilizing enhanced high spectral efficiency transceivers). However, it is only in the long-term scenario that C+L band systems (or, in limited cases, a full multi-band system) might be needed.

Moving on to the backbone network, a full multi-band system and/or SDM will be required in the long-term scenario (with limited deployments in the mid-term). Starting from the mid-term scenario, complete multi-band deployments (with or without SDM architecture) are recommended. Looking further ahead, a coordinated and coexistent coexistence between MB and SDM will be necessary to meet evolving network demands.

Regarding the development of the MB S-BVT transceiver, it is specifically designed for future 6G metro networks. It employs multi-carrier modulation and supports multiple transmission frequency bands. The prototype operates in the C and S bands using OFDM modulation. Ongoing optimization efforts include S-band amplification, programmable S-band filters, and improved tunable laser sources. An optimized prototype is expected to be generated by M30 of the project, further enhancing the performance and applicability of MB transmission systems.

The development of a flexible, high-capacity multi-frequency optical switching solution for B5G-OPEN networks is underway. This solution introduces a customizable MB-OADM designed to support various traffic requirements. The document discusses the practical deployment of MB-OADM in metropolitan access networks for aggregating X-haul traffic, showcasing its efficiency and low power consumption. Within this framework, optical integrated low-polarization-dependent Multi-Cast Switch chips and C+L band WSS chips have been designed to ensure seamless integration and performance in multi-frequency optical networks.

Simultaneously, the design and testing of multi-band optical amplifiers is progressing. This document highlights the importance of adjusting amplifier gain and tilt to achieve consistent OSNR across channels. It introduces forward control for optical amplifiers, emphasizing the role of pre-tilt in compensating power transfer within the transmission fiber. Additionally, the document underscores the advantages of Raman amplification in enhancing optical performance, particularly in the S-band.

Furthermore, a filter-less solution is presented with a specific focus on metropolitan aggregation network scenarios and their performance implications. It encompasses various network topologies and hardware optimizations, particularly related to traffic and sub-link aggregation. The document delves into the design and functionality of unfiltered drop nodes, highlighting their critical role in achieving multi-band scalability and emphasizing their importance in future networks. Additionally, the document discusses OSNR margin and successful prototype characterization, demonstrating effective add/drop functionality across different frequency bands.

B5G-OPEN proposes an architecture of the optical access network based on the integrated X-Haul options by employing the access planning tool introduced in D4.2. Furthermore, the LiFi technology in B5G-OPEN is enabled by an ecosystem of multi-user techniques, resource allocation algorithms, and security strategies. This deliverable provides a practical example of such a network, illustrating the seamless integration of LiFi technology into the broader network infrastructure.

Finally, the document delves into various monitoring techniques designed to enhance network surveillance and provide real-time performance data for effective anomaly detection and network management improvement. It explores a range of methods for optimizing optical network performance, including longitudinal power profile monitoring using coherent receivers, fiber loss anomaly localization through cross-phase modulation, and the application of P4 technology within packet-optical networks. These monitoring techniques play a crucial role in ensuring the efficient operation and management of advanced optical networks.

TABLE OF CONTENTS

TABLE OF CONTENTS	12
1 Introduction.....	1
2 Transport platform options	3
2.1 Network Architecture overview.....	3
2.2 Estimation of traffic needs in network segments	6
2.3 High capacity optical backbone node	9
2.4 Optical regional node	10
2.5 Optical hub node	12
2.6 Optical access node	14
3 Optical subsystems, switching and amplification	15
3.1 Transmission subsystems	15
3.1.1 Multiband S-BVT	15
3.1.2 Physical Layer design tool	19
3.2 Multiband optical switch	23
3.2.1 Multiband optical node architecture	23
3.2.2 2-degree RODAM in Metro-Access Network for Converged X-haul Traffic with OpenRODAM.....	24
3.2.3 Photonics Integrated Multi-cast selective switch.....	27
3.2.4 Photonics Integrated C+L Wavelength selective switch	28
3.3 Multiband amplification	29
3.3.1 Multiband amplifiers	29
3.3.2 Raman amplification	31
3.4 Filterless solutions	34
3.4.1 Performance analysis of metro-aggregation network scenarios	34
3.4.2 OADM FILTERLESS SOLUTIONS	37
3.4.3 Filter-less OADM upgrade strategies	39
3.4.4 (SEMI-)FILTER-LESS ADD/DROP NODE PROTOTYPE	40
4 Integrated Access and X-haul options.....	43
4.1 B5G-OPEN access network architecture.....	43
4.2 An Access Planning Tool	43
4.3 Lifi access.....	45
5 Packet and optical monitoring.....	48
5.1 Longitudinal power profile monitoring.....	48

5.1.1	Longitudinal Power Monitoring over a deployed 10,000-km Link	48
5.1.2	Locating Fiber Loss Anomalies with a Receiver-side Monitoring Algorithm exploiting Cross-Phase Modulation	49
5.2	Monitoring in Packet-Optical Networks	52
6	Prototypes development status and delivery	55
7	Conclusions.....	58
8	References.....	59

1 INTRODUCTION

This deliverable D3.2 “Second year results on data plane infrastructure” describes the activity related to work package 3 in the B5G-OPEN project. It identifies the context for the design and operation of multiband (MB) optical network across multiple segments, by enabling transmission within S and O bands in addition to current C + L bands. To meet this challenge, advanced technologies are required, and this deliverable reports on the packet-optical node architecture options being investigated in the project. A companion document investigating control and management architecture options is the deliverable D4.1.

The document covers the design and development of the optical continuum multiband data plane infrastructure incorporating heterogeneous nodes and transmission technologies. It encompasses multiple domains with different characteristics in terms of reach, capacity, cost, scalability, flexibility, etc. The objectives of this work package are:

- Design of an innovative optical transport infrastructure supporting MB connectivity and estimation of traffic needs in network segments.
- Design, prototyping and experimental assessment of the novel optical network devices for switching, amplification and transmission.
- Exploring and testing optical innovative solutions for MB PON, Point to Multi-point (PtMP) with low cost and power consumption for next-generation optical access & 5G X-haul.
- Design and testing the effective integration of fiber with LiFi systems supporting multi-cell simultaneous transmission for bandwidth maximization and effective hand-over.
- Design, prototyping and testing advanced monitoring solutions to enable efficient and flexible use of the infrastructure.

The D3.2 document gives the progress of work package 3 during the second year of activity of B5G-OPEN toward the above-mentioned objectives and is structured as follows:

Section 2 provides a comprehensive overview of the architectural and design considerations for optical nodes and transport systems across various network segments, including Backbone, Metro-Core, and Metro-Aggregation. It also discusses network topologies and central office architectures in different segments, evaluates traffic requirements, estimates optical node capacities, and provides preliminary characteristics for optical nodes across various layers.

Section 3 describes the B5G-OPEN optical data plane framework. In particular, the multiband sliceable bandwidth/bitrate variable transceiver (MB S-BVT), employs multicarrier modulation and offers flexibility by supporting various transmission bands. The Multiband ROADM based on SOA take advantage of dynamic reconfiguration, lossless operation, and low power consumption with photonic integration, and can be the critical component in Multiband optical Metro-Access Network. The optimization of Multiband amplification that achieves the consistent OSNR across all channels is presented. Moreover, a filterless solution has been investigated in the optical Metro-Aggregation networks.

Section 4 addresses the Integrated Access and X-Haul Options in the B5G-OPEN project. It outlines the project's network architecture, introduces an Access Planning Tool (B5G-ONP) for resource coordination, and presents LiFi access prototypes. The LiFi technology implementation is discussed, including key components like PHY, MAC, and optical front-end elements.

Section 5 advances in packet and optical monitoring, with a focus on longitudinal power profile monitoring using nonlinear back-propagation techniques. It introduces successful applications of nonlinear back-propagation techniques for monitoring long-distance power profiles, presents a cost-effective alternative to OTDR, and highlights a framework for in-network telemetry data processing. The section also covers a successful testbed deployment, showcasing its minimal impact on network performance and resilience improvements.

Section 6 reports the prototypes development and delivery and discusses the status, software control integration, roadmaps to complete, and delivery time.

Section 7 provides the conclusions to the document.

2 TRANSPORT PLATFORM OPTIONS

This section presents a general view of the architecture and design criteria of optical nodes and transport systems at different network segments: Backbone, Metro-Core and Metro-Aggregation, based on the list of requirements reported in Section 3.1 of D3.1, that are here updated considering mainly the estimations reported in [RUI23]. [RUI23] define three reference timeframe scenarios: short-term, mid-term and long-term (approximately 3, 6, and 9 years from now respectively) and for each of them gives some estimations of traffic demands in the different network segments.

Based on these estimations, indications are given on the introduction of new technologies and architectures at different network segments and in different timeframe scenarios. In Metro-Core and Backbone networks the deployment of C+L band systems, or SDM (e.g. multi parallel fibers) is foreseen starting from the short-term scenario, while in the Metro-Aggregation segment the currently deployed C-band will be sufficient to fulfill the requirements up to the mid-term scenario (leveraging enhanced high spectral efficient transmitters and receivers), and only in the long-term scenario C+L band systems (and in limited cases the full multiband systems), or SDM will be required. In the Metro-Core networks full multiband systems and/or SDM will be required in the long-term scenario (with limited deployments also in the mid-term scenario). A full multiband deployment (with or without an SDM architecture) will need to be deployed in the Backbone segment starting from the mid-term scenario, while in the long-term the synergy and co-existence of both full multiband technology and SDM will be required

An overview of the network topologies and the central office architectures in the different network segments is described in subsection 2.1. The evaluation of traffic needs, and a consequent estimation of optical nodes capacity at different layers, are reported in subsection 2.2. Based on these estimations, preliminary indications on the characteristics of the optical nodes at different layers are presented in the following subsections. These indications will be the basis of a more detailed design activity of node architectures that will be carried on during the third year of the project.

2.1 NETWORK ARCHITECTURE OVERVIEW

Figure 2-1 shows the B5G-Open reference network topology, highlighting the Metro-Core and Metro-Aggregation segment (Figure 2-1 (a)) and the Backbone segment (Figure 2-1 (b)).

The main characteristics of each segment in terms of number of nodes, average and longest path, types of transported services considering both the state of the art and the expected evolution and so on are detailed reported in D2.1, taking as a reference three of the main European operators’ networks.

As reported in D2.1, the Metro-Aggregation network is a collection of horseshoe topology networks terminated in pairs of hub Regional Node, collecting and delivering traffic from several Access Nodes.

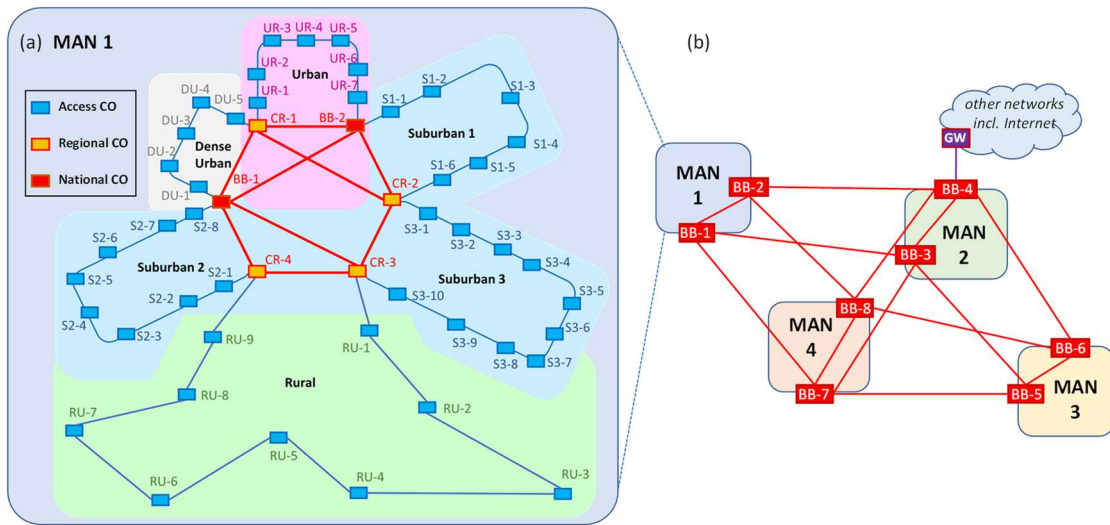


Figure 2-1 - Metro-Core and Metro-Aggregation reference network topology.

A key aspect of these horseshoe topology networks is that the uplink the traffic is collected from a number of access nodes and delivered to a single metro-aggregation node. On the downlink the traffic is sent from a single metro-node and delivered to several access nodes. This Point-to-MultiPoint (PtMP) architecture plays into the key strengths of the XR optics, which, unlike access PtMP solutions, has enough capacity (initially 400G), and can expand in the future to higher capacities by either using 800G XR systems, or stacking multiple 400G XR systems using DWDM.

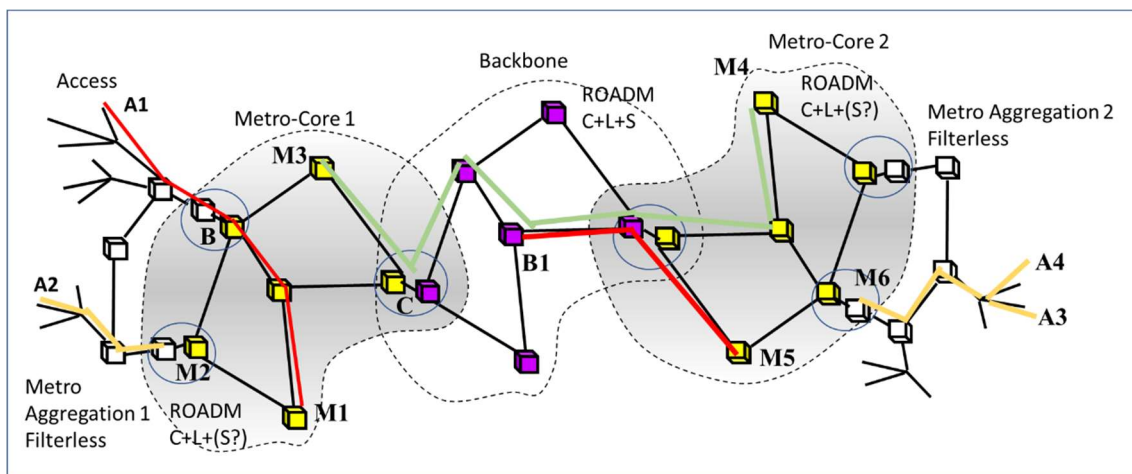


Figure 2-2 Continuum concept.

Another key concept considered by the B5G-OPEN project is the idea of optical continuum. Figure 2-2 shows a network divided into access, metro and backbone segments and illustrates this concept with simple graphic examples. At the left and right ends of the figure the yellow lines highlight optically transparent connections created between access terminals and the first aggregation nodes (A2 to M2, and A3/A4 to M6). The redline on the left instead represents a transparent optical circuit which, starting from the access (A1), reaches the first aggregation node (B) and then also the more internal metro-core node (M1). Finally, examples of optical continuity between a single metro-core network and the backbone are represented (red line in the center of the figure, from M5 to B1) or even an optical continuity between two nodes that are part of different metro-core networks that pass through the backbone (M3 to C, B1 and M4).

Those examples illustrated in the figure above are particularly significant situations for which B5G-OPEN is called upon to identify specific transmission, switching and control plane solutions.

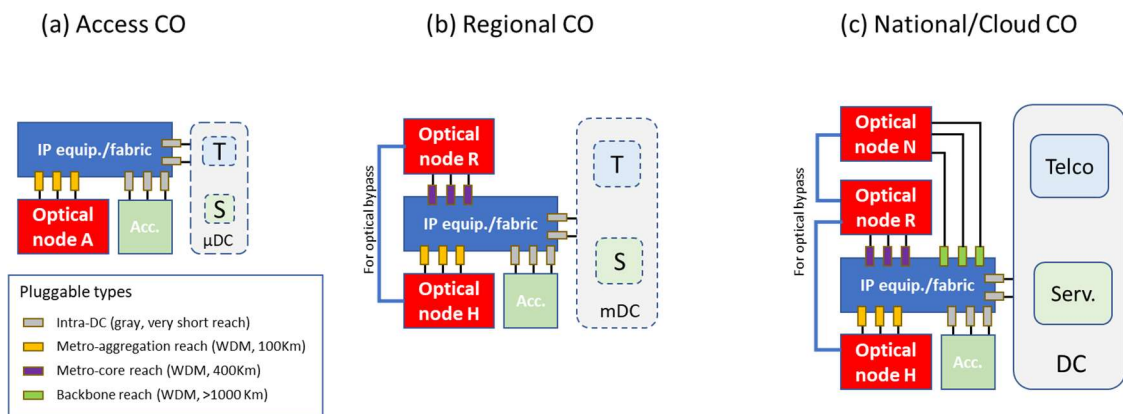


Figure 2-3 Central Office reference architectures. The optical nodes are highlighted with red boxes and, depending on their role in the hierarchy there are potentially four different types: Access (A), Hub (H), Regional (R), and National (N).

The Access CO (Figure 2-3 (a)) includes an optical access node (red box, Optical Node A), a packet node (blue box, typically a single piece of equipment, but it could be a structure with multiple devices, for example in a leaf & spine configuration). In case we consider decentralized architectures, a micro data center based on servers and switches that hosts telco functions (T) and possibly also service functions (S) is also included in the node. Access is represented by the green box which includes both fixed and mobile network access devices. For simplicity's sake, this representation does not give evidence of the possibility of an optical continuum between the access points (e.g., customer termination, OLTs or mobile stations) and COs of higher hierarchy level (Regional or National COs), but this possibility also exists as an architectural option that will be addressed with specific case studies. Similar architecture is for Regional and National/Cloud COs (Figure 2-3 (b), (c)) with optical, packet and data center equipment scaled up in size and power according to the hierarchical role of the CO. Optical Hub nodes (Optical node H) terminating metro aggregation segments, are included in both Regional and National/Cloud CO as, of course, both COs are usually terminating some aggregation network. They also may collect local access traffic. National/Cloud CO includes Optical National nodes (Optical node N) and often have also the role of Regional node thus including an Optical Regional node (Optical Node R). Optical bypass is shown explicit in Figure 2-3 (blue lines) as an interconnection between different hierarchical optical nodes in the same CO.

The rectangular modules inserted in the packet box are optical pluggable modules (transceivers) whose types are specified in the bottom left of the figure. The grey modules are compliant with very short reach used for intra-CO connections. The orange modules are inter-CO WDM pluggable modules with a reach sufficient to cover the metro-aggregation distances (up to 100 km). The violet pluggable modules have a reach sufficient to cover the metro-core distances (up to 400 km). The green modules are pluggable (but they can be replaced by a combination of a grey transceiver and a transponder) for inter-CO connections in the backbone. The green module has a reach which depend on the backbone extension (normally of the order of 1000 Km or more).

Figure 2-4 shows the Central Office reference architectures of Figure 2-3 mapped on B5G-OPEN high-level architecture (Figure 1.1 of B5G-OPEN Deliverable D2.1). From the bottom to the top

we can identify: the metro aggregation network (typically a horseshoe) made of Access COs hubbed to a couple of Regional COs; the metro core network (typically a mesh) interconnecting Regional COs together and with one or more Backbone COs; and the backbone (typically a mesh) interconnecting National COs together and with gateways for exchanging traffic with the outside (peer networks or the Internet). The DC in the national COs is always present while the presence and extent (i.e., capacity) of the micro and mini data center component on the access COs and on the regional COs will depend on the specific telco and service architectural solution (i.e., centralized, semi-distributed or distributed). This is the reason why the lines surrounding the micro and mini DCs in the access and regional COs are dashed. For example, a semi-distributed solution could have the mini DC only in the regional COs and not in the access CO where only packet and optical equipment would be present.

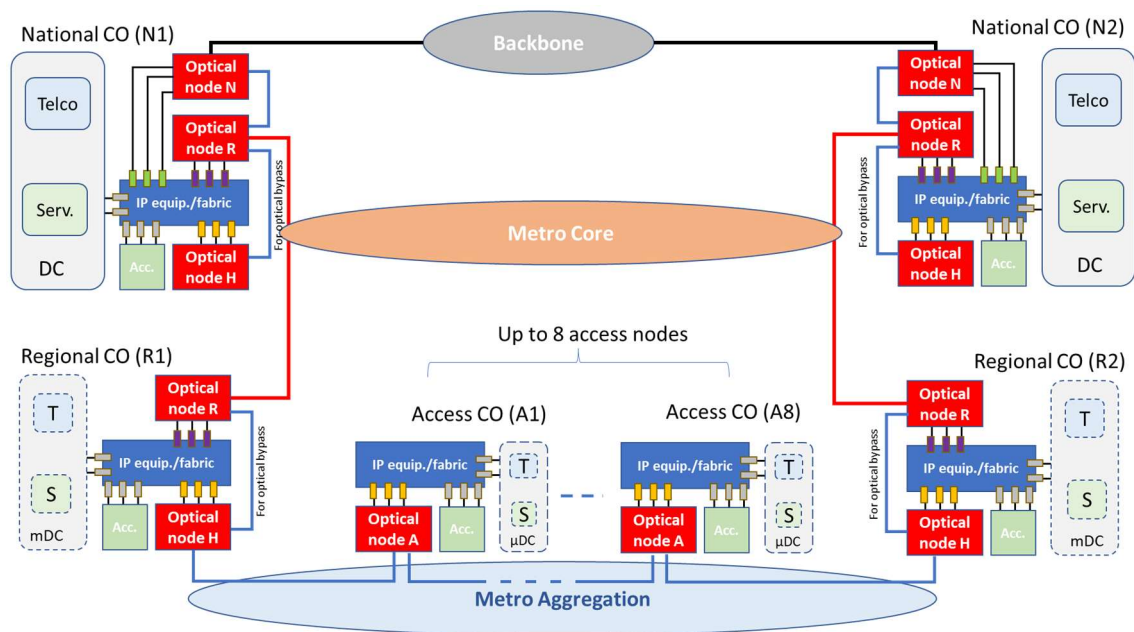


Figure 2-4 – Central Office reference architectures mapped on B5GOPEN high-level architecture.

2.2 ESTIMATION OF TRAFFIC NEEDS IN NETWORK SEGMENTS

Figure 2-5 highlights the traffic flows generated by an access node. The traffic flows can be potentially, under the hypothesis of centralized architecture (Telco and Service functions only at the National level), transported in optical continuity, by means of optical bypasses between the aggregation and the core segments, up to the first National level node. Other options are possible for a centralized architecture, for instance the optical circuits can be terminated in each network segment and traffic aggregation is done at the packet level. This traffic aggregation option guarantees efficiency in the case of small traffic compared to the granularities of the WDM circuits as well as it allows for statistical multiplexing of traffics coming from many sources.

In the lower part of Figure 2-5 is an aggregation structure (horseshoe topology) made of up to eight Access nodes (A1 and A8 are depicted, the other six are in between) and two hubs (R1 and R2).

The regional nodes (R1 and R2) are connected by a Metro Core network which also includes two National COs. National nodes (N1 and N2) are connected to the backbone for long distance traffic exchanges.

In case of centralized architecture, the traffic generated by an Access node must reach the National node to be processed. Figure 2-5 shows the flows exchanged by the access Node A1 and the national nodes N1 and N2.

It is reasonable to assume that there are two totally independent ways to reach two national node locations from the access node. The violet dashed lines represent the flows originating from node A1 that reach the nodes N1 and N2 passing respectively through nodes R1 and R2. The two flows carry 50% of the traffic in normal conditions (load sharing) or 100% of the traffic generated by node A1 when a fault occurs on one of the two physical paths from node A1 towards nodes N1 and N2. This simplified scheme is valid in the case of fixed routing but it is sufficiently accurate to evaluate the impact of traffic on the network even if the routing was dynamic and adaptive. Please note that for assuring the reach from Access CO to the National CO, and according to the legenda in bottom-left of Figure 2-3, the WDM pluggable must be of the violet type (reach 400 km), that is, it must be able to cross both the metro aggregation and metro core segments.

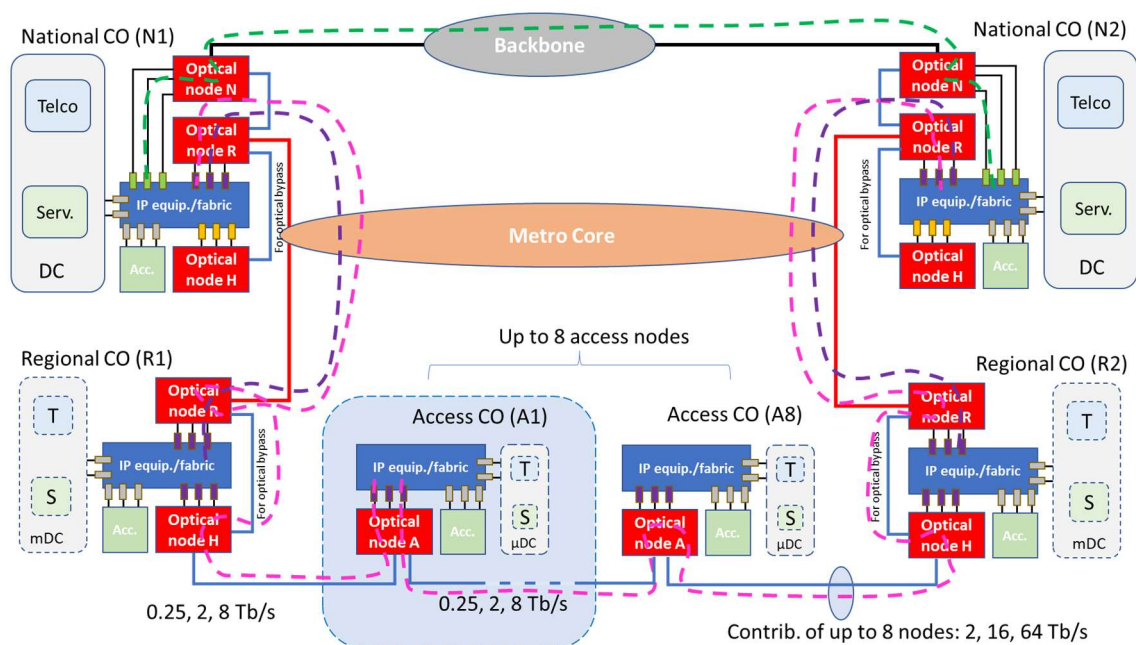


Figure 2-5 – Example of traffic flows generated a by an Access CO and crossing the network architecture for a centralized architecture and 100% of optical bypass between Access CO and National CO. A flow between National COs (green dotted lines) is also represented.

Having as a reference the traffic values generated by the access nodes reported in [RUI23], the impact of the traffic from access on the optical access nodes (Optical Node A) is shown in figure 2-5. The values reported here are for a node of dense urban geotype.

Each optical node of type A in the access CO has to add/drop 2×0.25 , 2×2 or 2×8 Tb/s traffic and handle up to 7×0.25 , 7×2 or 7×8 Tb/s of traffic in pass through in short-, medium- and long-term periods, respectively. This is true when the aggregation horseshoe is made of eight access nodes (plus two hubs) and the nodes are all of the high demanding dense urban traffic geotype, i.e., it's the worst case in terms of capacity demand in the aggregation segment.

This means that an optical access node (type A) should be capable to add and drop 2×0.25 , 2×2 or 2×8 Tb/s of traffic on the tributary side and handle a total of $16 \times 0.25 = 4$, $16 \times 2 = 32$, $16 \times 8 = 128$ Tb/s of traffic on the line side on the two node degrees. Each degree connects the node in

analysis to the adjacent optical node by a bidirectional link. The multiplying factor 16 is due to $7 \times 2 = 14$ pass through flows, two for each other access node in the horseshoe, plus 2 add/drop flows, one for each direction of the horseshoe.

Concerning the line systems in the horseshoes (link from node to node), it has to be capable of carrying the traffic contribution of up to 8 access nodes, that means, as shown in the bottom-left of Figure 2-5, 2, 16 and 64 Tb/s in short, medium and long term, respectively.

Looking at the hub optical nodes H, to evaluate the size of the node an assumption has to be made about the number of horseshoes collected by each hub and the number and the geotype of COs in each horseshoe. Each hub is assumed to collect 16 dense urban nodes that can be organized, for example, in 2 horseshoes of 8 nodes each, or in 4 horseshoes of 4 nodes each (or any other feasible combination of horseshoes whose total sum of access nodes is 16, for instance 3 horseshoes of 5, 7 and 4 access nodes respectively). Regional COs hosting Hub nodes are also assumed to be of dense urban geotype being a node capable of generating local traffic. Under this assumption the total traffic collected by the horseshoes doesn't change, while the number of nodal degrees depend on the number of horseshoes. A maximum number of 4 collected horseshoes is assumed.

With these numbers and assuming that all the traffic coming from the Access nodes is optically bypassed towards the metro core (this is true only for centralized solutions and if bypass is achievable taking into account the distances involved and available equipment, otherwise traffic is processed at packet level) the capacity of the optical node H has to be 0.25, 2 and 8 Tb/s in add/drop (local traffic, highlighted in violet dashed line) and 4.25, 34, 136 Tb/s on line side.

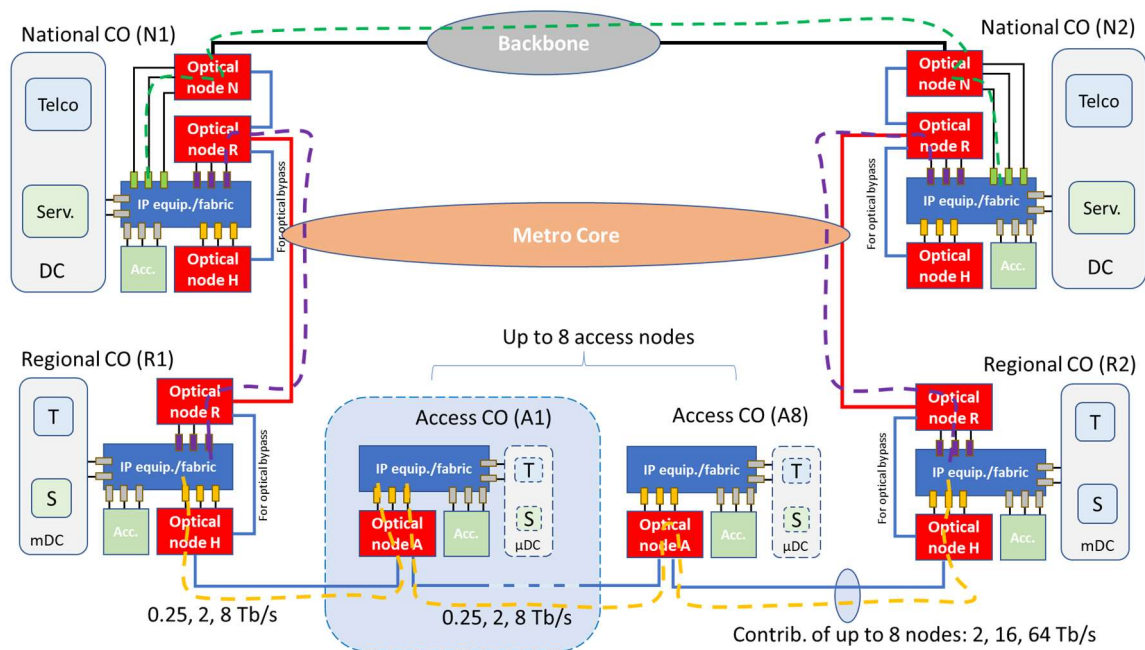


Figure 2-6 – Example of traffic flows generated a by an Access CO (orange dotted lines) and directed to Regional CO and aggregated flows from Regional CO to National CO (violet dotted lines) for a decentralized architecture and 0% of optical bypass between Access CO and National CO. Flows between National COs (green dotted lines) is also represented.

Another example is given in Figure 2-6 and relates to a decentralized architecture in which Telco and Service functions are positioned in the mini-DC at the regional CO. In this case, all the traffic collected in access is optically terminated in the regional node (orange flows and orange

pluggable modules which have a reach suitable for the metro aggregation segment). The aggregate traffic that has to be carried from the regional CO to the national CO (that is part of the traffic collected by access COs as a fraction of it is served on local DC) is carried by connections terminated in the optical nodes of type R in regional and in national COs (violet dashed lines). These connections require pluggable modules of violet type, i.e. modules with metro core reach. This example assumes that no traffic coming from Access CO is optically bypassed in the regional CO. However, hybrid schemes are also possible in which part of the traffic generated by access CO (e.g., 50%) is optically bypassed at regional CO and processed in a National CO, while the remaining part (the other 50%) is optically terminated and processed at regional CO. In this case the number of optical pluggable modules required is greater than the previous individual cases. . Indeed, the number of modules has to be doubled on the access COs since both the metro aggregation Reach (orange type, to reach the Regional CO and terminated on IP equipment there) and Metro Core Reach (purple type, to reach the national CO and terminated on IP there) pluggable module types are required. Furthermore, to achieve this hybrid scenario the access has to differentiate the traffic destined to the regional DC and the one destined to the national DC. This is assumed to be technically possible.

2.3 HIGH CAPACITY OPTICAL BACKBONE NODE

The requirement for a backbone network is made under very simplified assumptions and it considers the numbers already used in computing the requirements of Node R of a National CO (see Figure 2-10). Of the total traffic collected by the National CO (it includes traffic coming from optical nodes R of Regional COs gathered plus the traffic collected locally by Optical Node H) the 50% is assumed to be exchanged with the backbone (the other 50% is processed by local DC and terminated there).

It results that in the Optical Node the add/drop (A/D) traffic is 18.5 Tb/s, (50% of 37 Tb/s) in the short term, 148 Tb/s (50% of 296 Tb/s) in the medium term, and 592 Tb/s (50% of 1184 Tb/s) in the long term. Under the hypothesis that optical node N of a National CO is directly connected to other four optical nodes N in as many National COs and the pass-through traffic is twice (+200%) of the add/drop traffic, the resulting numbers of capacity on link and add drop interfaces are as in Figure 2-7.

These hypotheses are extremely simplified, but they give the idea of how big a national node could be. The variations can be in the number of nodal degrees (less or greater than 4, but not by much), the unbalance of the load in the various directions (different than uniform as in the example) and in the dimensions of the node which can be much smaller for peripheral nodes or

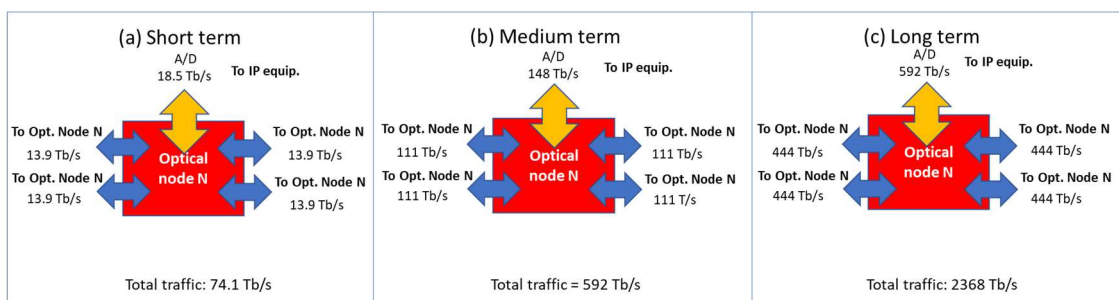


Figure 2-7 – Connectivity and traffic requirements of Optical Node N in National CO in short, medium and long term. The numbers are valid under the hypothesis of nodal degree 4, traffic balanced in the various directions and percentage and component of pass through equal to double that of add and drop traffic.

larger for nodes hosting gateways. A more in-depth analysis is beyond the scope of this deliverable and the numbers provided in the figure can be considered sufficient as a specification for the national level optical nodes to be considered in B5GOPEN.

2.4 OPTICAL REGIONAL NODE

To calculate the requirements of a type R optical node it is necessary to make some assumptions on the number of nodes, on the structure of the metro core segment network, and on the percentage of the traffic generated by the access nodes that is brought to the national COs. This percentage is assumed to be equal to 50% (this implies that the architecture is semi-distributed or distributed and 50% of the traffic is served at the Regional or Access Node level). The following analyses is to be considered purely indicative and could change with other network topologies and other hypotheses of network functions degree of centralization.

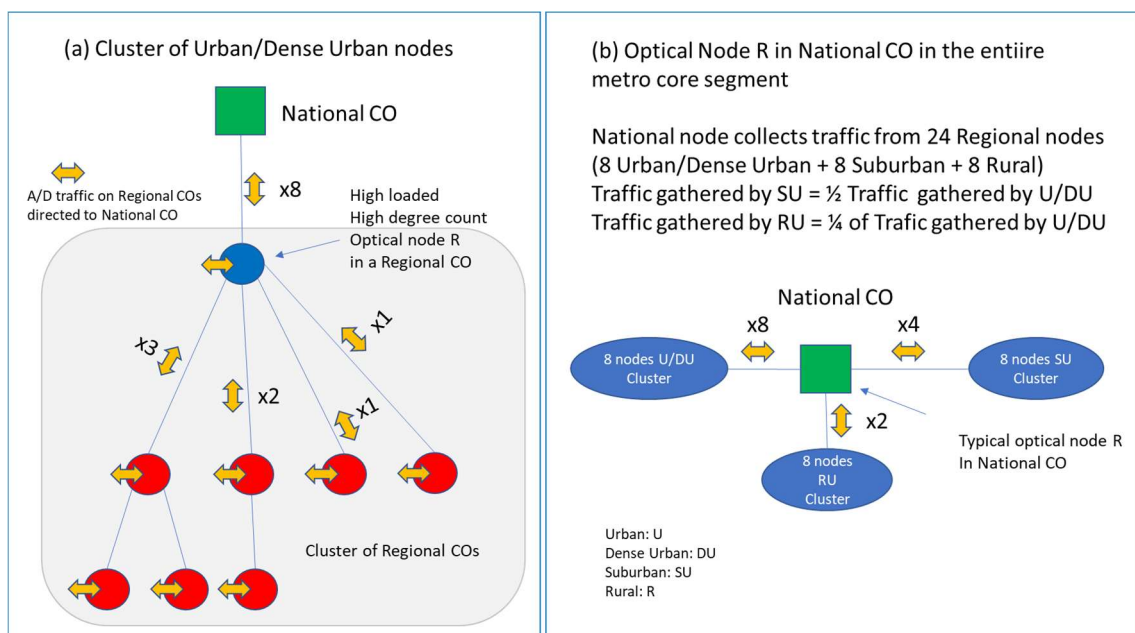


Figure 2-8 – Assumptions made on connectivity and traffic of an high loaded optical node R in Regional CO which collect and forward traffic in a cluster of Regional COs (a) and in a typical optical node R in National CO collecting traffic from three cluster of Regional COs (b).

The most critical situation for the optical node R in Regional CO occurs when the node is directly connected to a National CO and acts as a transit to other nodes. In Figure 2-8 (a) the optical node R in blue is located in a Regional CO and acts as a transit for other 7 nodes to bring traffic to the optical node R located in the national level CO. Assuming that all the nodes are of the same Geotype (e.g., Dense Urban) and the amount of traffic generated by a Regional CO and directed to National CO is the same for all Regional CO, the requirements in terms of topological degrees, and traffic on add/drop blocks and lines is given in Figure 2-9 for the short (a), medium (b) and long term (c) periods. The traffic values reported in the figure include the traffic generated in access by the users and conveyed up to the core metro network segment, where it is assumed that each regional CO on average collects traffic of ten Access COs. However, there are other traffic needs not considered such as alignment traffic of the mini DCs. The alignment traffic is the traffic that the DCs exchange to keep the stored information consistent and for all the necessary updates to guarantee uniformity of the service in all the locations of the network where there are DC components. The alignment should be significantly lower than the customer

traffic and therefore the values shown in the figure can be considered adequate to estimate the demand for a type R optical node in regional COs.

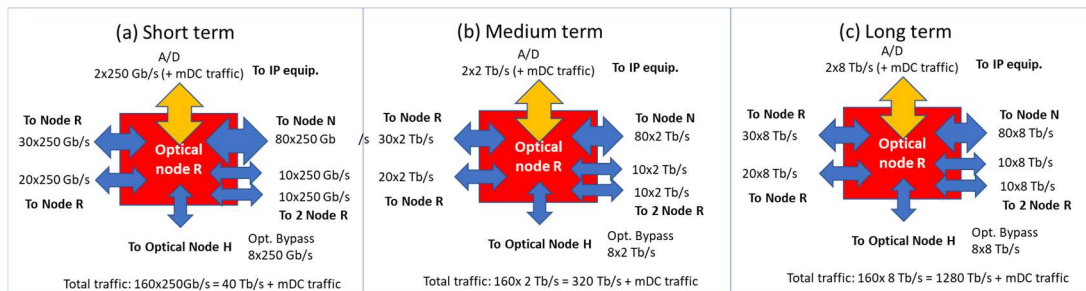


Figure 2-9 – Connectivity and traffic requirements of Optical Node R in Regional CO in short, medium and long term.

To obtain the requirements of an R node that is part of a National CO node, it is necessary to make an assumption on the pool of nodes collected by the national node. Figure 2-8 (b) shows a case in which an optical node R located in a National CO collects the traffic generated in the core metro segment on three connection links, each one connecting an optical node R located in a regional COs.

For simplicity, each of the links aggregates the traffic of a cluster of homogeneous nodes which in this case are: a cluster of eight urban or dense urban nodes (the one used to evaluate the requirements of the optical node R of the regional CO case in Figure 2-9), a cluster of eight suburban nodes and a cluster of eight rural nodes. It was also assumed that the traffic generated by the suburban cluster is half of the urban cluster, and the traffic of the rural cluster is equal to a quarter of the urban one (see Figure 2-8 (b)).

Under these hypotheses the requirements in terms of connectivity of the type R optical node in the National CO for the three time periods are shown in Figure 2-10.

It can be observed that the optical node R has quite different requirements in the Regional CO and the National CO. In the Regional CO the number of line degrees required is equal to 6 compared to the 4 required in the National CO. However, given the same number of total nodes and traffic conveyed on the National CO, if the Regional CO clusters were smaller and higher in number, the number of line degrees of optical nodes R in the National CO could rise, probably up to 6 (or even more), as for the optical node R in the Regional CO.

For what concern the total traffic to be switched, it is noted that in the National CO the values are approximately double compared to the optical node R with the highest requirements in the Regional CO as shown in Figure 2-9 (e.g., 75 Tb/s instead of 40 Tb/s, for the short term).

Finally, another important difference between the two optical nodes of type R is in the percentage of add/drop traffic compared to the total traffic. In the optical nodes R hosted in the Regional COs, and in particular those directly connected to the National COs, the add and drop traffic is much reduced compared to the traffic on the lines that connect the other nodes. This is due to the numerous simple transit flows destined to the National CO. In optical nodes located at the termination point of traffic processing in the data center (DC), it's worth noting that the add, drop, and line traffic are effectively balanced.

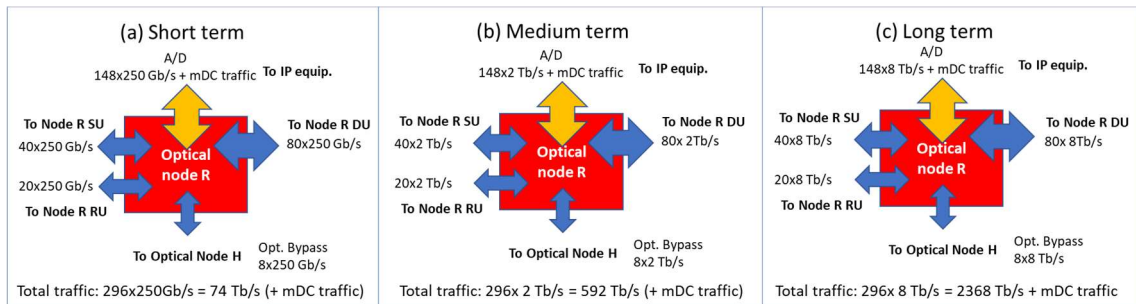


Figure 2-10– Connectivity and traffic requirements of Optical Node R in National CO in short, medium and long term.

2.5 OPTICAL HUB NODE

The connectivity and traffic requirements for the optical node H that is hosted in the Regional COs for three different conditions in terms of percentage of optically added/dropped traffic in the node are shown in Figure 2-11, Figure 2-12 and Figure 2-13. In the examples two horseshoes and a total of 16 optical access nodes (optical node A) are collected by each optical node H. The same traffic requirement holds also for a greater number of collected horseshoes. The main difference is only in the nodal degree count (one nodal degree per collected horseshoe is necessary) and in the partitioning of the total traffic collected from 16 optical access nodes between the nodal degrees. As mentioned above, a hub node is expected to collect a maximum of 4 horseshoes.

Figure 2-11 shows the condition when all the traffic collected by the hub node from the Access nodes is forwarded directly, through an optical bypass line connection, to the optical node R and then forwarded outside the Regional CO (towards other Regional or National COs). This is the typical condition when the Telco functions are centralized (located at National COs) and the traffic does not need to be processed at the packet level in the Regional node. Depending on the optical devices performance, traffic coming from the aggregation has or not to be regenerated before to be forwarded in the metro core segment. This can be considered an extreme situation and if there was actually no need for add/drop, the optical node H could collapse into the optical node R and the Regional CO could be equipped with a single optical switch which performs both a collection function on the aggregation segment as well as a networking function on the core segment. However, the collapse of the H and R optical nodes on the Regional CO could be constrained by the required nodal degrees on the collapsed node, given that the H node still offers a consolidation capacity of the optical circuits from the aggregation lines towards the bypass connection. This is the more critical as the number of collected horseshoes increases.

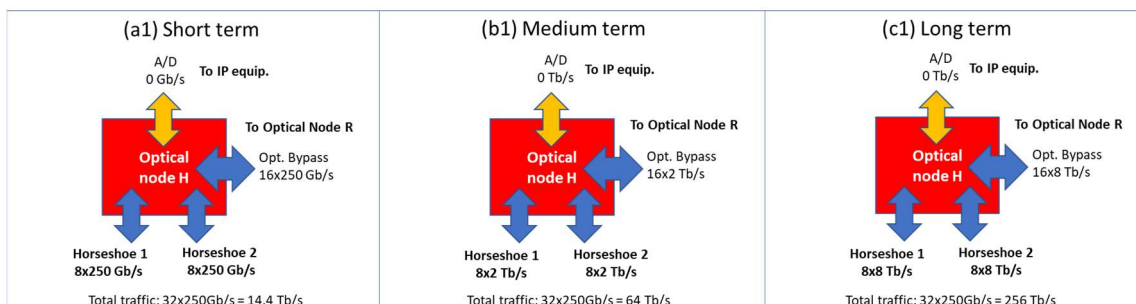


Figure 2-11 – Connectivity and traffic requirements of Optical Node H (Regional CO) in short, medium and long term for 100% of bypassed traffic.

Figure 2-12 shows an intermediate condition when 50% of the traffic is added/dropped in Regional CO to be processed at IP level, while the other 50% is forwarded through an optical bypass line connection, to the optical node R to be forwarded outside the Regional Node. This is the case of a semi-distributed scenario with Telco functions and services available on regional nodes and it is assumed that a part of the traffic (50%) is processed by functions at the level of that regional node, while the remaining part (50%) is forwarded to others regional or national nodes directly at the optical level. This hypothesis presupposes the ability of the access node to discriminate the traffic to be processed in the regional attestation node (the Regional CO where the optical node H is hosted) and the traffic to be processed in other regional nodes or at the national level. The two types of traffics will be transported with distinct optical connections.

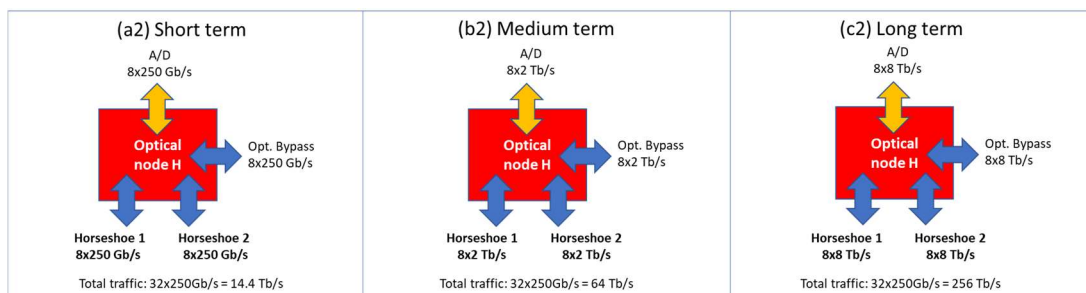


Figure 2-12 – Connectivity and traffic requirements of Optical Node H (Regional CO) in short, medium and long term for 50% of optically bypassed traffic.

Lastly, Figure 2-13 shows the situation in which the traffic collected by the optical node H is completely added/dropped to the regional node, i.e. there is no bypass traffic between optical node H and optical node R. It is the typical situation in which the network functions are present at the regional node (semi-distributed or distributed scenario) and all the traffic is processed in that node by the Telco functions before to be forwarded to the final destination which can be local (co-located mini DC) or remote (other regional or national nodes). Another scenario that could involve 100% add/drop of the traffic on the optical node H is when, even if the traffic must continue beyond the node in the core metro network, an aggregation and consolidation of the flows at the IP level is carried out before its transportation on the optical metro core network.

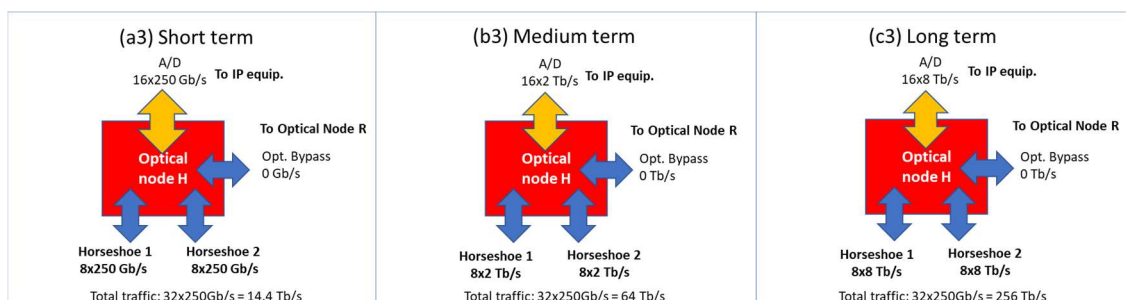


Figure 2-13 – Connectivity and traffic requirements of Optical Node H (Regional CO) in short, medium and long term for 0% of bypassed traffic.

The three situations represented above are indicative and constitute upper bound in each indicated time period as the largest number of A optical nodes (16) and dense urban type have been considered. In urban contexts, suburban, rural or mixed, H-type optical nodes may require much lower total capacities (a half or even a quarter of the indicated capacities may be a reasonable scaling factor in such cases).

2.6 OPTICAL ACCESS NODE

The connectivity and traffic requirements for the type A optical node hosted in the Access COs for the short, medium and long term are shown in Figure 2-14 (a), (b) and (c), respectively. The node is part of a linear horseshoe structure and requires only two nodal degrees (East - E - and West - W - in the figure) and an add and drop structure. The total traffic switched by the node (add/drop and line) is also reported on the bottom of the node box.

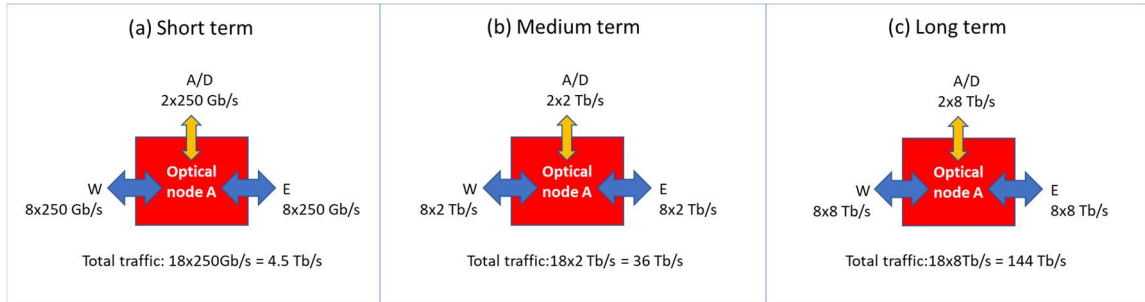


Figure 2-14 – Connectivity and traffic requirements of Optical Node A (Access CO) in the short, medium, and long term.

It should be noted that the traffic collected and switched by the optical nodes A in the figures above is that of dense urban type exchanges (the node itself and the other 7 connected in the same horseshoe). In urban, suburban, rural or mixed contexts, type A optical nodes may require much lower capacities (a half or even a quarter of the indicated capacities may be reasonable scaling factors in such cases).

3 OPTICAL SUBSYSTEMS, SWITCHING AND AMPLIFICATION

This section focuses on the design, prototyping, and experimental evaluation of innovative optical network devices tailored for functions such as switching, amplification, and filterless solutions in optical network.

Section 3.1 highlights the development of the MB S-BVT in the B5G-OPEN project. This transceiver, designed for future 6G networks, employs multicarrier modulation and supports multiple transmission bands, with a prototype operating in the C- and S-bands using OFDM modulation. Ongoing optimization efforts, including S-band amplification, a programmable S-band filter, and an improved tunable laser source, are expected to result in an optimized prototype by M30 of the project. The section also introduces a design tool for evaluating multi-band transmission systems, addressing issues like stimulated Raman scattering and power allocation across different bands for optimal performance.

Section 3.2 details the development of flexible, high-capacity multiband optical switching solutions for B5G networks. It introduces the customizable MB-OADM designed to support various traffic demands. The practical deployment of the MB-OADM in a Metro-Access Network for Converged X-haul Traffic is discussed, showcasing its efficiency with low power penalties. The section also highlights the low polarization-dependent MCS and the advanced C+L band WSS for filtered Metro-Access architectures.

Section 3.3 focuses on multiband amplification optimization in optical transmission systems, emphasizing the need to adjust optical amplifier gain and tilt for consistent OSNR across channels. It introduces feedforward control of optical amplifiers, highlighting pre-tilt's role in power transfer compensation within the transmission fiber. The section discusses ongoing multiband amplification research and highlights the advantages of Raman amplification in enhancing optical performance, especially in the S-band.

Section 3.4 explores filterless solutions in optical networks, with a focus on metro-aggregation network scenarios and their performance implications. It covers different network topologies and hardware optimizations, especially concerning traffic and sublink aggregation. The section delves into the design and capabilities of filterless add/drop nodes for multiband scalability and their importance in future networks. It discusses OSNR margin and successful prototype characterization, demonstrating add/drop capabilities across various bands.

3.1 TRANSMISSION SUBSYSTEMS

3.1.1 Multiband S-BVT

Within the B5G-OPEN project a multiband sliceable bandwidth/bitrate variable transceiver (MB S-BVT) is designed and implemented towards supporting the stringent requirements that 6G networks will pose in terms of capacity scaling, performance and efficiency. The MB S-BVT architecture based on multicarrier modulation (MCM) consists of multiple building blocks (bitrate/bandwidth variable transceivers, BVTs) that can work in different transmission bands (i.e. C-, L-, S-, O-, E- and U-bands) by adopting the suitable optical devices including tunable laser sources, modulators, amplifiers, filters and photodetectors. Mainly, the adopted implementation for the MB S-BVT prototype is based on external modulation and direct detection in order to simplify the transceiver architecture while maximizing cost-efficiency,

making the metro aggregation context its main target. A flexible combination of the different building blocks is achieved thanks to the envisioned transceiver architecture, also enabling point-to-point (PtP) and PtMP transmission. Specifically, the different slices/contributions of the BVTs, composing the S-BVT, are aggregated and distributed by including a MB optical aggregator/distributor to efficiently generate a high-capacity flow, which can be demultiplexed, at some point of the network, distributing the different S-BVT slices to different network end-points. Sliceability is a key feature of the transceiver that enhances overall network flexibility and adaptability.

Prototype description: The MB S-BVT prototype, built by CTTC within B5G-OPEN, consists of 2 slices operating at the C- and S-bands, as depicted in Figure 3-1.

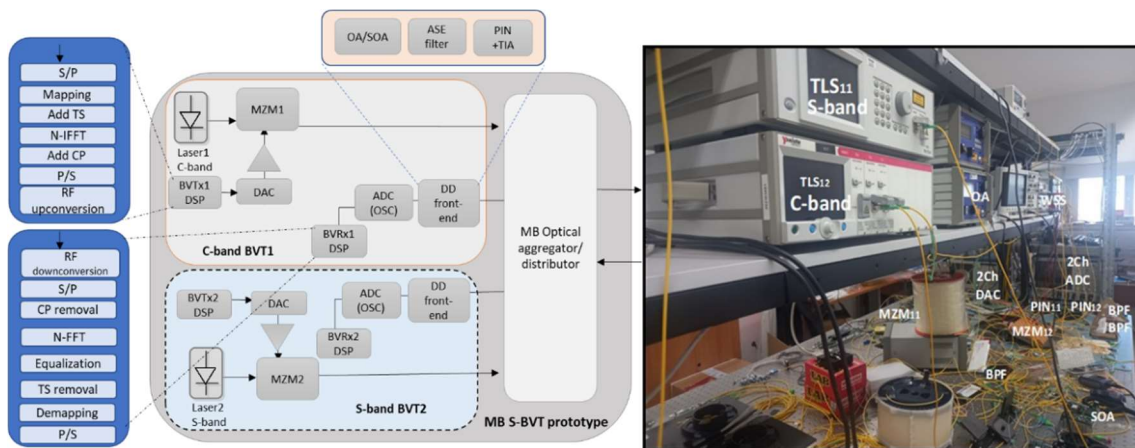


Figure 3-1 – MB S-BVT architecture and lab prototype.

The DSP of the MB-SBVT is based on offline processing, where orthogonal frequency division multiplexing (OFDM) modulation is implemented also enabling the use of bit/power loading (BPL) techniques to further enhance overall system's flexibility and performance. According to the channel profile, different power values and modulation schemes can be adopted at the subcarrier level [Nad22]. At the DSP transmitter side, additional processes take place, such as data mapping and parallelization, training symbol insertion, Inverse Fast Fourier Transform (IFFT) implementation, cyclic prefix insertion, serialisation, and RF up-conversion. At the DSP receiver side, RF downconversion, data parallelization, CP removal, fast Fourier transform (FFT) implementation, equalisation, symbol demapping, and serialization operations are performed. The prototype transmitter front-end includes a high-speed DAC, operating at 64 GSa/s, and two MZMs, operating at the quadrature point to create the OFDM signals. Then a MB optical aggregator is included based on a MB passive band pass filter (BPF) to create a high-capacity flow, which can be transmitted through the network. Additionally, programmable filters such as wavelength selective switches (WSSs) can be used to perform single side band (SSB) modulation towards enhancing robustness against chromatic dispersion (CD) when transmitting over the fiber. The receiver MB S-BVT prototype, based on DD, consists of a MB BPF, to perform the distribution of the two MB slices, and an amplification and filtering stage followed by a PIN photodetector per slice. An EDFA and a WSS (ASE filtering), for the C-band contribution, and a SOA and BPF, for the S-band, are considered to properly amplify and filter each band/slice. The prototype also uses an oscilloscope (OSC) working at 100 GSa/s to perform analog-to-digital conversion. The programmability of the prototype is also enabled by implementing an OpenConfig SDN agent to reconfigure and program the different MB S-BVT parameters and

elements (i.e. DAC channels enabling/disabling, TLS optical power and central wavelength) according to the network needs and demand [Nad23].

Table 3-1 MB S-BVT prototype capabilities and target features/SPECS

MB S-BVT prototype capabilities	Target features/SPECS
MB operation	C+S transmission
Slice-ability	2 slices
Reach adaptability	B2B-75 km (MB transmission)
Capacity adaptability	10Gb/s-65 Gb/s per slice
Programmability	Laser central wavelength (TLS); Laser output power; DAC channels enabling/disabling (OpenConfig SDN agent)
Flexibility	PtP and PtMP operation; Adaptive loading

Prototype development status: A preliminary MB S-BVT has been implemented and a proof of concept assessment has been performed at CTTC premises as summarized below in this section. Currently, the MB S-BVT prototype is being optimized by considering S-band amplification based on TDFA with lower noise factor than SOAs. Also, it is considered the use of a programmable S-band filter, at the transmitter side, to perform SSB. Finally, a more stable TLS will be included in the prototype, to generate the S-band contribution, enabling higher output power values (which will relax amplification gain requirements) and enhanced performance.

Delivery time: It is expected to perform the update and assessment of the MB S-BVT and integration with the augment of the SDN OpenConfig agent at the beginning of the third year of the project targeting an optimized prototype towards the middle of the third year (around M30).

Preliminary proof of Concept assessment:

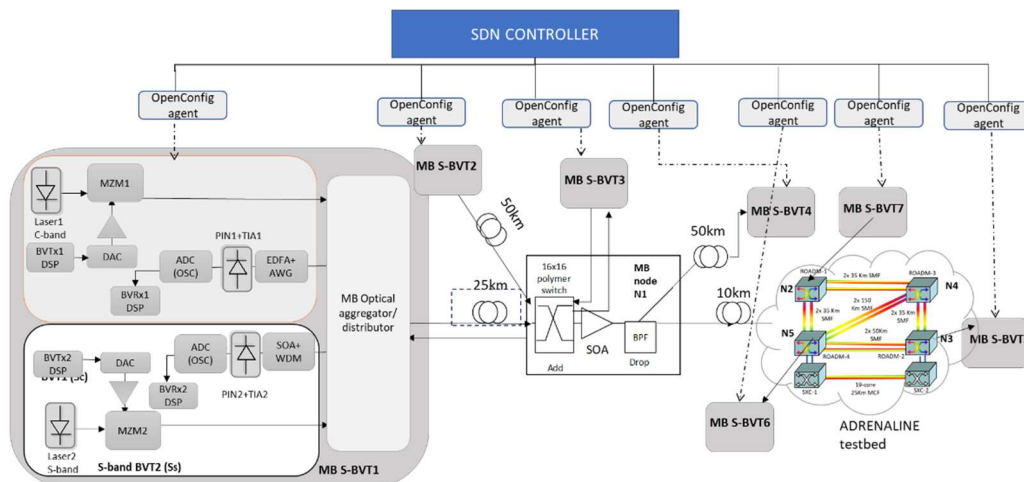


Figure 3-2 – Experimental setup.

For the preliminary proof-of-concept assessment, depicted in Figure 3-2, the TLSes composing the MB S-BVT prototype are set to 1550.12 nm (for the C-band slice, S_c) and 1500 nm (for the S-band slice, S_s). For the C-band assessment both DSB and SSB implementations have been evaluated, considering two different transceiver implementations (S-BVT1 and S-BVT3, respectively). SSB can be performed, by including a WSS as part of the MB optical aggregator

device. For the S-band only DSB has been performed. A hard-decision forward error correction (HD-FEC) threshold of 7% overhead is considered corresponding to a target bit error rate (BER) of 4.62×10^{-3} .

Table 3-2 Experimental results considering different network scenarios

Scenario	Band(s)	Rate (Gb/s)	# of hops	Length (km)	Path	BER
1	C+S	65 (SSB Sc); 65 (DSB Ss)	0	0	B2B	$3e-3$ (Sc); $4.6e-3$ (Ss)
2	C+S	48 (SSB Sc); 42 (DSB Ss)	1	25	SBVT1-SBVT3	$4.6e-3$ (Sc); $4e-3$ (Ss)
3	C+S	40 (SSB Sc); 26.5 (DSB Ss)	1	50	SBVT2-SBVT3	$3.5e-3$ (Sc); $4e-3$ (Ss)
4	C+S	29.3(SSB Sc);15.5 (DSB Ss)	2	75	SBVT1-SBVT4 and SBVT2	$4.6e-3$ (Sc); $4e-3$ (Ss)
5	C	30 (DSB Sc)	1	10	SBVT3-SBVT5	$2.7e-5$
6	C	30 (DSB Sc)	2	60	SBVT3-SBVT6	$2e-3$
7	C	30 (DSB Sc)	3	95	SBVT3-	$4.65e-3$

Different scenarios for a metro-regional aggregation network, detailed in Table 3-2, have been identified and assessed to evaluate MB transmission performance and sliceability/scalability over a MB network. A 16x16 polymer switch photonic integrated circuit (PIC) prototype, which can also support spatial granularities, a semiconductor optical amplifier (SOA) and a BPF are included in the setup to emulate a MB node (N1) [Hyu20]. The ADRENALINE testbed has been included for the assessment of the C-band contribution. Specifically, the ADRENALINE testbed is an open disaggregated SDN/network function virtualization (NFV)-enabled packet/optical transport network and edge/cloud computing infrastructure for beyond 5G, 6G and IoT/vehicle-to-everything (V2X) services [Mun17]. The ADRENALINE photonic mesh network includes 4 nodes (2 reconfigurable optical add/drop multiplexers, ROADMs and 2 optical cross connects, OXCs), 5 bidirectional flexi/fixed-grid dense wavelength division multiplexed amplified optical links up to 150 km (overall 600 km of optical fiber) and 1 passive optical network with a 19-core 25 Km multi core fiber (MCF) and bundles of SMFs. The main achieved results are also reported in Table 3-2 achieving a maximum aggregated capacity of 130 Gb/s (in back-to-back, B2B) ensuring the target BER. On the other hand, 45 Gb/s MB transmission is demonstrated up to 2-hops path of 75 km. The C-band contribution can be distributed through the ADRENALINE testbed ensuring 30Gb/s after a 3-hops path of 95km. Regarding scalability, thanks to the modular and scalable transceiver approach, additional building blocks/slices can be enabled working at different bands beyond the C-band, according to the network condition and requirements. 21.6 Tb/s transmission can be envisioned considering 160 C-band channels of 25 GHz (SSB) and 175 S-band channels of 50 GHz (DSB).

3.1.2 Physical Layer design tool

The physical layer (transmission) performance evaluation tool assesses physical layer performance in the context of transmission systems with Multiple Optical Bands. It is tailored to estimate the physical layer performance of terrestrial fiber-optic European national networks.

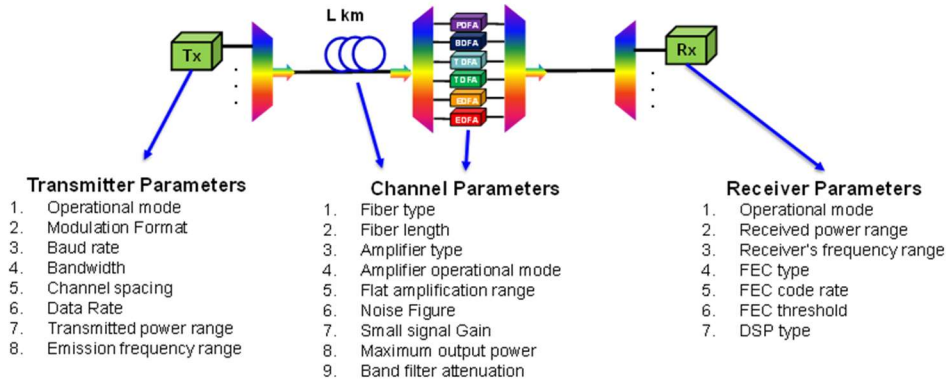


Figure 3-3 – The system-level parameters taken as input.

Figure 3-3 illustrates the system level input parameters for the estimation of the physical layer performance of a Metro/Core point-to-point link. The physical layer phenomena taken into account are ASE accumulation, intra-band nonlinearity (FWM) and inter-band nonlinearity (SRS). Because of the latter, there is power transfer from the lowest wavelength channels to the higher wavelength channels in the spectrum leading to an uneven power distribution (tilt) at the output of each span that accumulates with the number of fibre spans as in Figure 3-4.

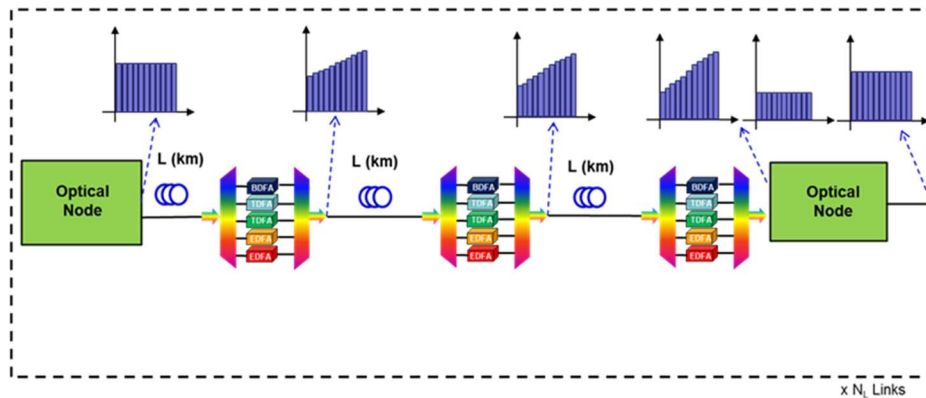


Figure 3-4 - Gain/power tilt due to SRS and compensation.

To compensate this effect in the particular tool implementation, WSS-based optical nodes are assumed every third span that compensate for this tilt, so all channels enter the fiber of the next link with the same nominal power level (Figure 3-4).

The details of the physical layer modelling used by the tool have been presented in D3.1. Here we present some newer results on the validation of the SRS model and the optimization methodology used.

3.1.2.1 Validation of the SRS Model

The initial validation results of the spectrally extended SRS model were shown in D3.1, benchmarking the closed-form abstract model against a commercially available simulation tool (VPI). The latter employs the Split Step Fourier Method (SSF) to numerically solve the

corresponding nonlinear propagation equations in an optical fiber by making use of the true Raman spectrum.

Here we provide further evidence for the validity of this formalism by presenting the results from simulations with systems a) having a higher number of channels; and b) with a wider range of values for the total power traversing the fiber link.

The function of merit against which the benchmarking is made is the quantity G_{SRS} , which estimates the gain (or the depletion) in channel’s power at the end of a single link due to the SRS effect. With reference to Figure 3-3, the link consists of a fiber span plus the corresponding multi-band amplification stage. In the latter, the different xDFA terminals are individually regulated so their gain just compensates for the losses due to propagation along the preceding fiber span plus the losses due to the band mux/demux which were assumed to be of the order of 2 dB. The G_{SRS} is ratio of the output power, as measured at the output of the band multiplexer which is the zero (gain x loss) point for the combined losses, over the launch power for a single channel. By excluding the impact of all other non-linear effects, the higher/lower channel power that is estimated/measured at the output of the link is due to SRS.

We consider two multi-band transmission systems/scenarios with 305 Nyquist channels in total (with 61 channels per band) and 505 Nyquist channels in total (with 101 channels per band) in E, S, C and L-bands. Each channel is operated at a 100G line-rate with 32 Gbaud source rate and a QPSK modulation format. We consider a single link of 50 km in length with the parameters of Table 2 for the central wavelength (λ) of each band, the values for the fiber attenuation (α), dispersion (D), nonlinear coefficient (γ), effective area (A_{eff}) per band and noise figure (NF) of the different amplifiers (see Table 3-3), as these fiber parameters are wavelength dependent. To compensate for the losses, xDFA amplifiers are used with characteristics as in [Uzu21a]: a Bismuth-DFA for the E–band while the S band is segregated in two sub-bands (S_1 -band and S_2 -band) to ensure the corresponding amplifiers provide sufficient power per channel [Uzu21b] so two separate Thulium-DFAs are used for the S_1 and S_2 -bands. Finally, two Erbium-DFAs are optimized for the C and L bands. The values of the corresponding NFs are as in [Uzu21a]. By means of these parameters, the G_{SRS} is always estimated for the central channel in each band.

Table 3-3 The Parameters of the Multi Band Transmission Systems

	E band	S_1 band	S_2 band	C band	L band
λ (nm) -central	1416.5	1466.7	1496.7	1546.9	1594.6
α (dB/km)	0.280	0.246	0.229	0.211	0.210
D (ps/nm/km)	8.63	12.06	13.97	16.96	19.60
γ (1/W/km)	1.65	1.50	1.44	1.32	1.24
A_{eff} (μm^2)	70	74	76	80	83
NF (dB)	6	5.5	5.5	5.5	6

Regarding the numerical simulation tool, the following parameters were used: the fiber type was the “universal” one to ensure that the power exchange due to SRS between any pair of channels across the entire spectrum, from the E to the L band, is accounted for in all cases; the “sample-mode bandwidth” is set for 32.7 THz while 8,192 bits were used per polarization. The wavelength-dependent physical layer parameters of Table 3-3 e.g. α , D , A_{eff} , were manually inserted using text files. The remaining configuration parameters of the link were the following: at the end of each fiber segment, a “WDM_DEMUX” is inserted to split the spectrum in bands

so each band is amplified separately. This demux had “rectangular” shaped filters, while the “WDM_MUX” module which is placed in tandem mirrors the demux (see Figure 3-3). Under these specifications, for a system with 305 channels across the E, S, C and L-bands, the spectrum is as in Figure 3-5.

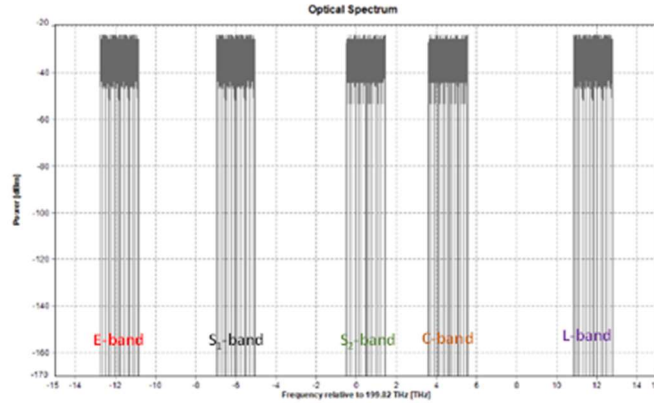


Figure 3-5 – The spectrum with 305 channels across the E, S, C and L-bands.

To calculate the G_{SRS} in the context of the numerical simulation tool, we measured the optical power of each channel at fiber input which was then compared against the power at the output of the band multiplexer.

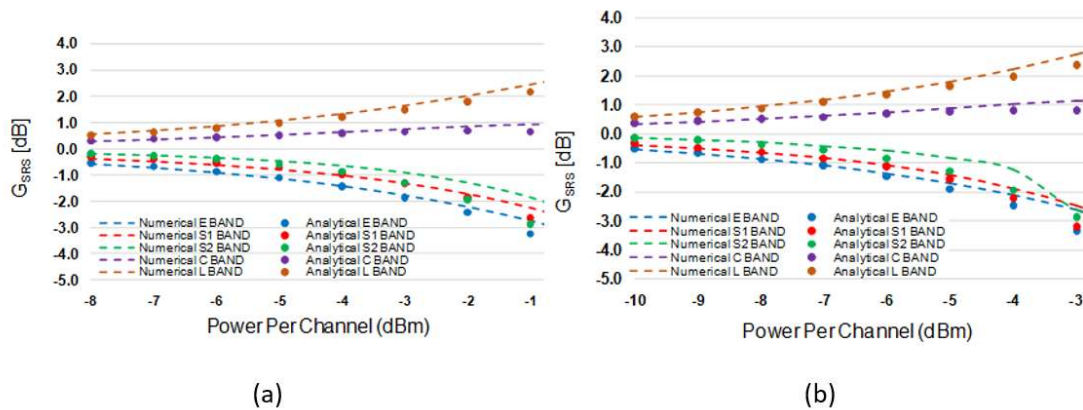


Figure 3-6 – Benchmarking of the spectrally extended SRS model using the G_{SRS} vs. power per channel against the corresponding numerical results for a 50 km link with (a) 305 channels; and (b) 505 channels.

In Figure 3-6 (a) and (b) we benchmark the G_{SRS} vs. P_{ch} values from the analytical and the numerical tools for a multi-band system with 305 channels and 505 channels in total, respectively. In particular, in Figure 3-6 (a) the launch power is iterated from -8 dBm per channel to -1 dBm and in Figure 3-6 (b) from -8 dBm per channel to -3 dBm per channel, respectively, values that correspond to a total optical power in the fiber of the order of ~250 mW. It is important to point out that all channels are simultaneously set to the same power level as the power is iterated at the system’s ingress.

For both systems in Figure 3-6, the maximum deviation between the analytical and the numerical methods is of the order of 1 dB when the total power in the fiber is up to +24 dBm. These findings are in-line with the limits set on the allowable total power within a fiber segment for the corresponding transmission system to operate in the weak-nonlinearity regime.

Evidently, from Figure 3-6 the impact of the SRS for a single fiber span becomes increasingly critical as the number of channels in the system and/or the power per channel increases. As a result, considerable power is transferred from E- and S-bands to L and C-bands as the number of cascaded fiber segment increases.

3.1.2.2 Multi-Band launch power optimization

The results of Figure 3-6 were obtained under the hypothesis that all channels in all bands are launched at the same power level. Although this is a reasonable assumption when the quest is to pinpoint the physical phenomenon of SRS in isolation, it is a sub-optimal method to deduce the operational conditions in the context of a PLI-aware RMSA algorithm where other linear and nonlinear phenomena contribute too to the final performance.

The approach we adopt here is to treat the different $P_{ch, \{band\}}$, representing the power all channels in a bands are launched, are used as free variables of a co-optimization that tailors the OSNIR performance per band. Our method manifests a very good balance between complexity and accuracy, it applies to an arbitrary number of bands, while not requiring frequent adjustments and tweaks of the corresponding optical amplifiers. The optimization algorithm in our case is based on simulated annealing [Kir83], and is shown below:

```

Initialize Pch per band values;
Set E = current system energy;
Set T = start temperature;
while T > end temperature do
  Modify one band's Pch value;
  Set E' = current system energy;
  Set ΔE = E' - E;
  if ΔE < 0 or e-ΔE / (K * T) > some uniform random
  number
    Set E = E';
  else
    Undo earlier Pch modification;
  end if
  Multiply T by the cooling rate;
end while

```

Algorithm 3-1 optimization algorithm

In our case the system's energy is given by

$$E = \sum_{band} \frac{C_{band}}{(OSNIR_{band})^2} \quad (3 - 1)$$

Where the $OSNIR_{band}$ values are calculated using the physical layer impairment model presented in D3.1, while the constants C_{band} allow us to tune the OSNIR performance per band. Two possible OSNIR tuning schemes are:

- 'flat' (less than 1-dB) variation across the entire E-band to L-band spectrum. This is made possible by trading the OSNIR performance in C and L bands in favor of E and L bands.

- ‘step-like’ where the OSNIR performance in some bands is maximized at the expense of the performance in the remaining ones. This is interesting in case some bands are used for shorter-length connections only.

Given that the physical layer impairment model internally works with a discrimination of the power levels down to the individual channel, this approach can be further expanded towards a more fine-grained power optimization, partitioning each band in smaller segments. Moreover, this optimization is applicable for an arbitrary number of channels per band.

3.2 MULTIBAND OPTICAL SWITCH

3.2.1 Multiband optical node architecture

In Task 3.2 of B5G-OPEN, we conducted investigations into new multiband optical switching solutions. These multiband optical switches are designed to operate across multiple bands, including the O-, S-, C-, and L-bands. This approach offers increased flexibility and higher capacity for B5G-OPEN networks, aligning with the stringent requirements of Beyond 5G (B5G) in terms of bandwidth, capacity, flexibility, and efficiency, all while maintaining transparent operation.

The node is equipped with a highly flexible multiband optical add/drop multiplexer (MB-OADM), which serves the purpose of adding, dropping, and bypassing traffic between Metro-Access and Metro-Core (metro aggregation segment). The schematic of the multiband optical network architecture, depicting the primary functional optical building blocks, can be found in Figure 3-7. The modular design of the MB-OADM building blocks allows for efficient customization based on various factors, including traffic volume, the number of channels, channel granularity, the number of bands, and the number of ports (or the degree of the switch). Our primary focus has been on the design and implementation of a programmable multiband optical add/drop multiplexer (MB-OADM) multiband wavelength selective switch (WSS), and programmable multi-cast selective switch (MCS) capable of operating across the O-, S-, C-, and L-bands, enabling seamless drop and continue operations.

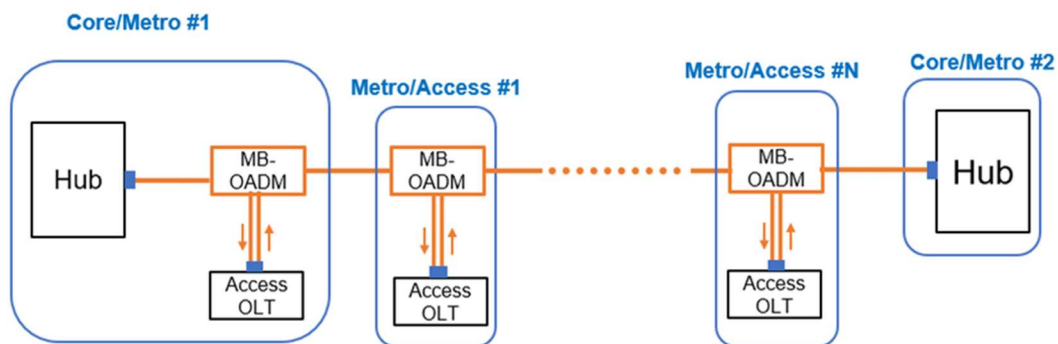


Figure 3-7 – Optical network architecture based on MB-OADM in Metro-Access and Metro-Core Network.

As shown in the Figure 3-8, we designed MB-OADM node based on a high-speed multi-band WDM architecture within the Metro-Access.

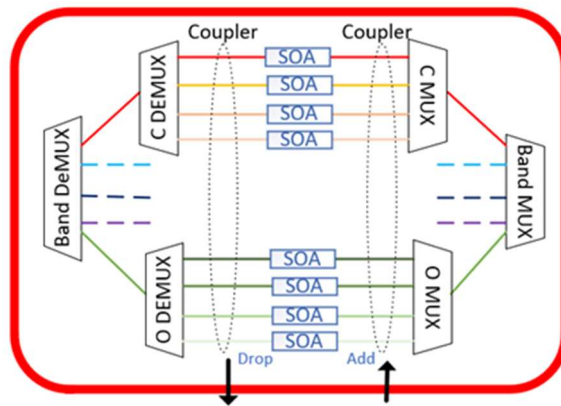


Figure 3-8 – MB-OADM Node architecture.

The MB-OADM Node consists of a band demultiplexer and multiplexer used to separate and combine the input MB signals. Commercial fused fiber WDM splitters can be utilized to implement the band demultiplexer/multiplexer. After separating the bands, each band's signals are directed to the respective OADMs operating at O-, S-, C-, and L-bands.

Each OADM is comprised of a demultiplexer, which separates the single-band signals into individual channels, an array of Semiconductor Optical Amplifiers (SOAs) that selectively and dynamically block or pass each channel, and a multiplexer for combining the channels. The drop stages are realized by a 3 dB splitter before each SOA, and the add stages are realized by a 3 dB combiner after the SOA and before the multiplexing stages. The SOAs compensate for the losses introduced by the muxes/demuxes as well as the 3 dB splitter/combiner.

It's worth noting that each SOA operates with a single channel, avoiding FWM (Four-Wave Mixing), XGM (Cross-Gain Modulation), and XPM (Cross-Phase Modulation) nonlinearities that can degrade signal quality. This implementation allows for the drop/add and continue operation of each individual channel.

Moreover, the modular architecture permits expansion in a 'pay-as-you-grow' approach to accommodate increasing traffic demands by processing multiple bands. Each module can handle the data channels of one of the multibands, starting from the C-band and subsequently expanding to the L-band, S-band, or O-band if needed. This design ensures a future-proof architecture capable of supporting traffic growth even in long-term scenarios.

3.2.2 2-degree RODAM in Metro-Access Network for Converged X-haul Traffic with OpenRODAM

To validate the operation of the MB-OADM, we conducted an experiment using the MB-OADM prototype, which operates in the O- and C-bands within a Metro-Access Network designed for Converged X-haul Traffic scenarios. This node was deployed in a metro-access network scenario to support X-haul traffic with varying Split function of 2, 7.2, and 8.

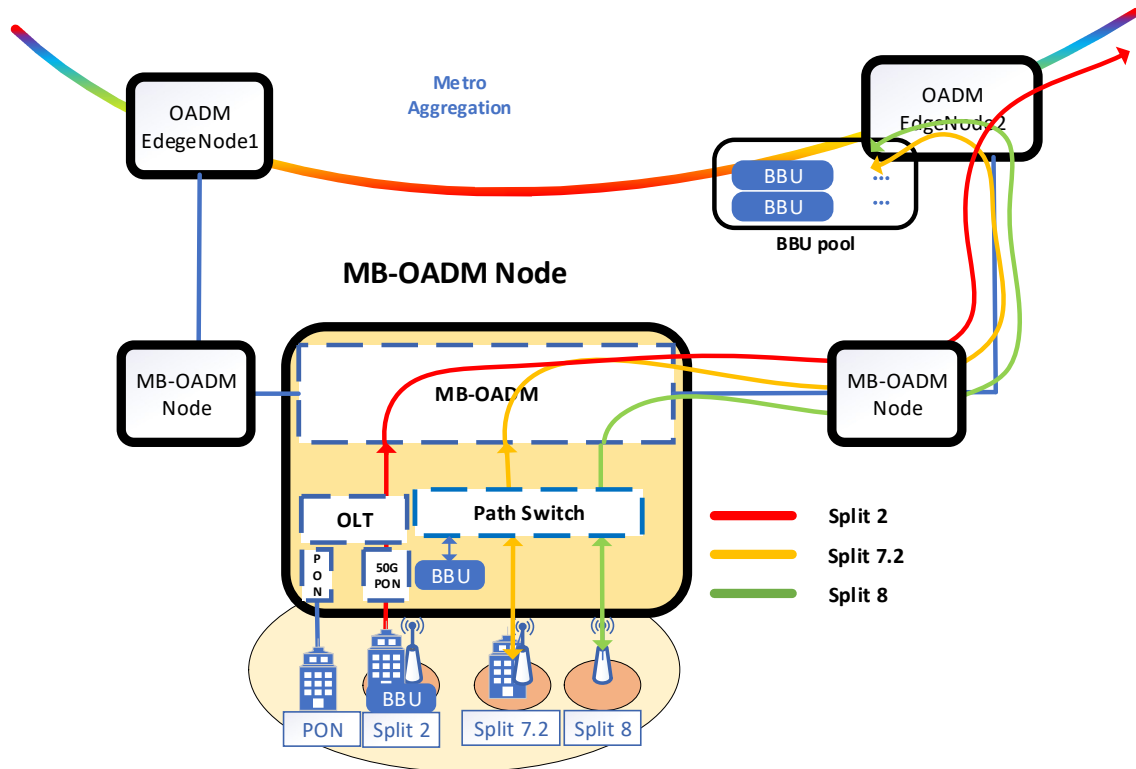


Figure 3-9 – Optical network architecture for converged X-haul.

The optical network architecture designed to accommodate converged X-haul traffic and support the three typical split function options is depicted in Figure 3-9. This network is structured around a horseshoe topology, leveraging flexible MB-OADM (Multi-Band Optical Add-Drop Multiplexer) technology.

In this architecture, each MB-OADM node is equipped with an MB-OADM capable of adding or dropping wavelength channels. The node control utilizes a fixed wavelength to carry out SDN control functions. The Optical Line Terminal (OLT) is responsible for aggregating Split 2 and PON (Passive Optical Network) traffic. To efficiently handle Split 7.2 and 8 high-speed data flows, a path switch is employed. This switch provides flexibility in allocating these data flows, allowing the data either bypass to the BBU (Baseband Unit) pool or be processed at the local BBU, depending on their latency requirements and type of traffic (mobile-related need to go through BBU others not). The OADM Node is designed to support data streams with varying capacity and latency requirements, which greatly benefit from the multi-band operation and rapid switching capabilities of the node.

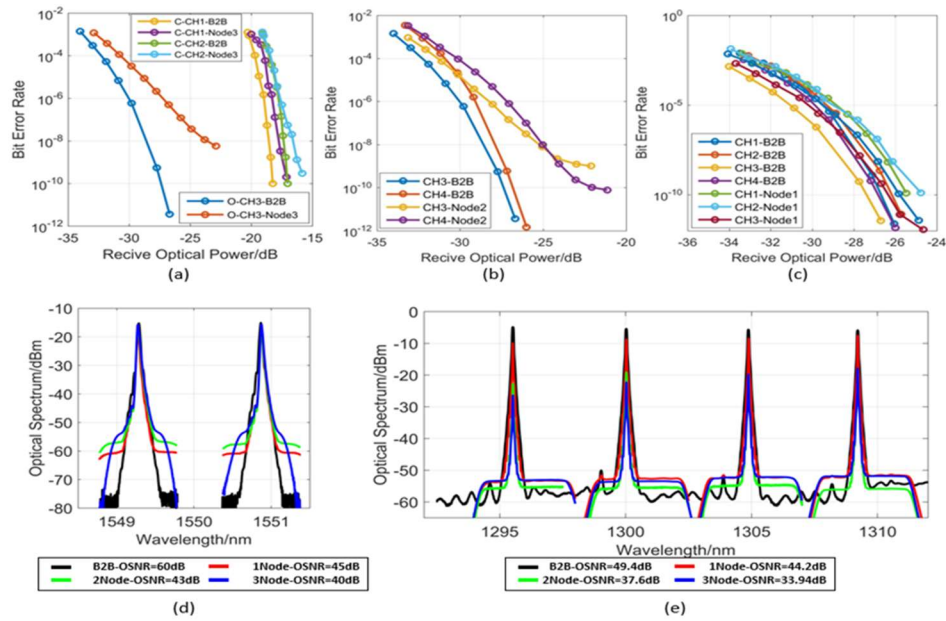


Figure 3-10 – BER results: a) Split 2; b) Split 7.2; c) Split 8. OSA: d) O-band receive optical spectra e) C-band receive optical spectra.

Figure 3-10 presents the experimental results for various scenarios. In the Split 2 scenario, we utilized O-band 25 Gbps for CH3, or alternatively, two C-band 10 Gbps channels, CH1 and CH2, for transmission. As shown in Figure 3-10 (a), the power penalty for CH3 after passing through three nodes was less than 5 dB, primarily due to reduced SNR. Figure 3-10 (e) illustrates an OSNR of approximately 24 dB for this channel after traversing three nodes. For the transmitted Split 2 flow on the C-band, the power penalty for CH1 and CH2 after three nodes was only 1.2 dB.

In the Split 7.2 scenario, we utilized CH3 and CH4 for transmission. Figure 3-10 (b) shows that after passing through two nodes, CH3 and CH4 exhibited power penalties of 4 dB and 3.69 dB, respectively. The OSNR after three nodes was around 28 dB.

For Split 8, we employed CH1-4 for 4x25 Gbps signal transmission. As depicted in Figure 3-10 (c), the power penalty for CH1-4 after passing through a node was found to be 1.14 dB, 1.11 dB, 0.95 dB, and 1.6 dB, respectively. The OSNR decreased from 49.4 dB in the Back-to-Back (B2B) configuration to 42 dB. Moreover, Figure 3-10 (d) and Figure 3-10 (e) display the optical spectra at different nodes, indicating that the SOAs in the nodes effectively compensate for the losses introduced by the MB-OADM and fiber link losses in the horseshoe network.

The experimental results underscore the versatility of the MB-OADM, as it can efficiently accommodate different splitting functions and data rates while maintaining low power penalties [XIA23]. Specifically, when configured for Split 8, the MB-OADM achieves a Bit Error Rate (BER) of less than 10⁻⁹ with a power penalty of under 1.6 dB. In the case of Split 7.2, it delivers a BER of less than 10⁻⁹ with a power penalty of less than 4 dB, even after traversing two medium-distance nodes. Lastly, for Split 2, the MB-OADM attains a BER of less than 10⁻⁹ with a power penalty of less than 5 dB in the O-band and less than 1.3 dB in the C-band, even after passing through three nodes in the access network. The results confirm that expanding the OADM for other bands in the low-loss window is feasible, given the wideband operation of the O- and C-band SOAs and the availability of SOAs with peak gain in other bands. Our future work is to

expand the MB-OADM operation to the S-band and L-band as well as assess it at higher data rates.

3.2.3 Photonics Integrated Multi-cast selective switch

For the filterless architecture within the Metro-Access Network, as depicted in Figure 3-11, the Access architecture employs high-speed coherent transceivers to allocate subcarriers for point to multipoint operation and traffic distribution. Furthermore, upstream and downstream data are transmitted through two separate optical fiber (Figure 3-11 (a)). In the downstream link, we employ SOAs for power compensation to counteract signal attenuation over long-distance transmissions. In the upstream link, ensuring the proper demodulation of each subcarrier requires power balancing. Therefore, prior to transmitting the upstream signal, power compensation is applied to the signal from the preceding node, followed by early compensation for transmission losses through a BOOST-type SOA.

Since each node serves by four subcarrier, we've introduced a multicast selective switch in both the transmitter and receiver sections to accommodate a broader range of users. This switch plays a crucial role as optical bypass and amplifier of the uploaded and downloaded signals from the access. Therefore, it is important to design multicast and select (MCS) switches that can expand the number of users by controlling different optical paths.

We have designed a low polarization-dependent MCS based on a recently developed bulk SOA that has been co-integrated with passive waveguides. The distinctive feature of our proposed MCS switch lies in its utilization of this innovative bulk SOA, which requires the co-integration of active SOAs, including gate and booster elements, with several passive InP (Indium Phosphide) components.

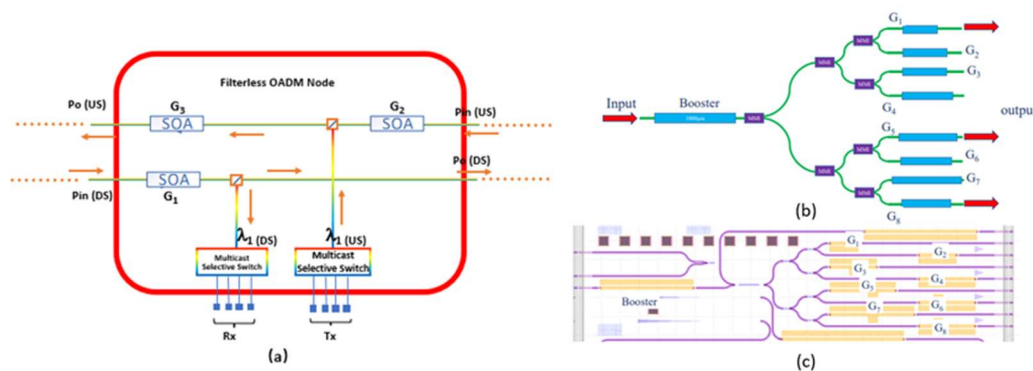


Figure 3-11 – (a) Filterless OADM Node architecture (b) Schematic of the low PDG bulk SOA co-integrated with butt-coupled waveguides. (c) The Mask design.

Figure 3-11 (b) presents the block diagram of our 1x8 WDM MCS switch. This configuration consists of nine active SOAs, with one serving as a booster and the remaining eight acting as optical gates. To connect the booster with the gates, we employ Multi-Mode Interference (MMI) devices, which serve as power splitters/combiners. The connections are made using a combination of passive straight and curved waveguides. Within the booster, the input signal undergoes amplification, and the amplified signal's power is then split and distributed to the eight SOA gates through three stages of cascaded 1x2 MMIs. At each of these eight SOA-based gates, the optical signal can either pass through or be blocked, depending on the applied on/off current.

Figure 3-11 (c) provides insight into the mask design, which is 1mm×4.6mm. The SOA gate lengths vary between 300 μm and 900 μm to enable a comparison of output optical power, bandwidth, and polarization-insensitive functionality across the MCS switch under varying SOA lengths. To preserve the SOA's performance, anti-reflection coating is applied to the chip's facets to minimize reflections. To ensure manufacturing reliability, the spacing between the gate SOAs is consistently maintained at 250 μm.

3.2.4 Photonics Integrated C+L Wavelength selective switch

For the Filtered architecture within the Metro-Aggregation Network, we also investigate and fabricate a C+L band wavelength selective switch. The PIC WSS architecture is shown in Figure 3-12. The chip architecture features a single input port that branches into eight WDM modules or WSS, each of which has eight output ports. Each WDM module processes eight channels spaced 400 GHz apart. The module includes an SOA followed by an AWG demultiplexer that separates the WDM channels, and an array of SOAs. A second AWG serves as a multiplexer. In total, the module includes three cascaded MMI splitters that split the input signal to feed other WSS modules on the chip, and one MMI on the input port and one MMI on the output port for alternative routing. Therefore, each channel of every WDM module contains one booster SOA, one gate SOA, five MMIs, and 2 AWGs, from input to output.

This photonic technology is based on SOAs to provide fast switching for mux/demux, loss-less operation, high contrast ratio and low channel cross-talk. The PIC can select one or multiple wavelength channels and forward the channels to the output ports according to the switching control signals. Turning ON/OFF the SOAs determines which wavelength channel is forwarded to the output or is blocked. The broadband operation of the SOAs enables the operation with any wavelength, whereas the cyclic AWGs allow the PIC to work in dual band. Moreover, the amplification provided by the SOA compensates the loss introduced by the two AWGs and five MMIs. The designed chip is InP material-based wafer and all 8 WSS together occupies the space of two generic InP cells, with each cell measuring 4.6×4 mm². This means that each WSS module occupies one-fourth of a single cell.

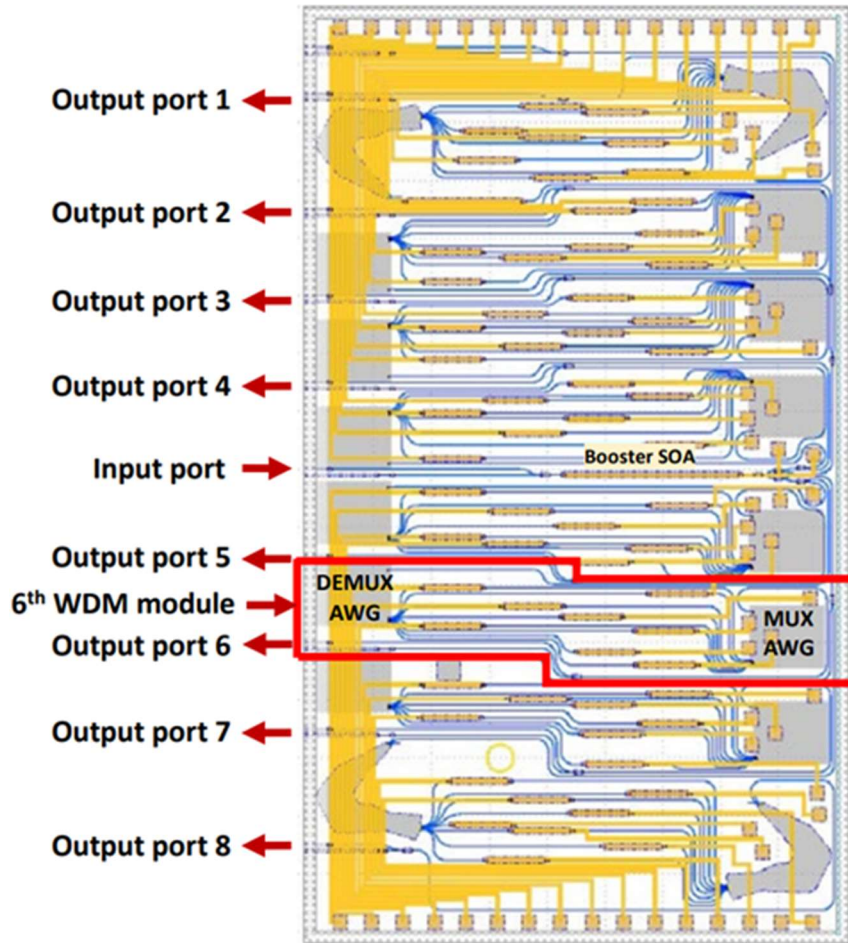


Figure 3-12 – The Mask design sample of 1X8 C+L band WSS.

In summary, our exploration has focused on the development of cutting-edge multiband optical switching technologies, including a programmable MB-OADM, a low polarization-dependent MCS, and a C+L band 1×8 WSS. These breakthroughs are finely tuned to address the demands of B5G networks, delivering enhanced capacity and flexibility while ensuring transparent operation across various frequency bands. We've demonstrated the practical implementation and versatility of the 2-degree MB-ROADM, showcasing its efficiency in handling diverse split functions and data rates with minimal power penalties. Moreover, the MCS, featuring a unique bulk SOA design, exhibits low polarization-dependent gain and wide bandwidth support.

3.3 MULTIBAND AMPLIFICATION

3.3.1 Multiband amplifiers

Currently used optical transmission systems make use of a single wavelength band only and the average per channel power of installed rare-earth doped fiber amplifiers does not change in case of a channel drop. In other words, the gain of an amplifier averaged over wavelength remains constant. However, this is no longer the case in systems making use of several wavelength bands and using individual amplifiers by band. In fact, the optimum average gain and the optimum pre-tilt of the individual amplifiers change with the channel drop. The key problem addressed in this

document is how to adjust the gain and the tilt of optical amplifiers in multiband systems such that the OSNR of all channels is almost equal.

First WDM systems transmitting signals in two wavelength bands have been developed already two decades ago. However, these systems have been designed for point-to-point data transmission and they did not support optical networking. Therefore, transient control has not been an issue at this time and there was no need to develop corresponding control architectures. With improved spectral efficiencies achieved by using more complex modulation formats and the further improvement of forward error correction (FEC) codes, there has no longer been a need for supporting several wavelength bands when optical networks have been introduced. In the meantime, transmitting data via several wavelength bands is reconsidered since further increasing the spectral efficiency without significantly decreasing the maximum reach has become difficult. Therefore, research activities on multiband transmission has been started.

Feedforward control of optical amplifiers helps to avoid strong transients in optical networks mainly in case of channel drops. Such channel drops lead to a reduction of the power transfer among the wavelength channels in the transmission fiber due to SRS. Equal optical signal-to-noise (OSNR) ratio at the receivers is typically achieved by introducing a pre-tilt into the spectrum at the output of each amplifier. This pre-tilt compensates for the power transfer in the transmission fiber such that all channels have equal power at the end of the span.

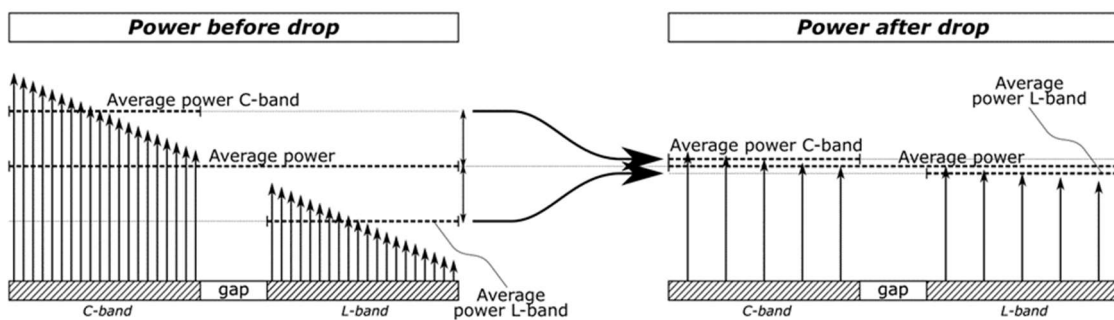


Figure 3-13 Steady-state power spectrum at the input of an optical fiber before and after a drop of channels.

Adapting the average channel power individually per wavelength band in case of a channel drop improves transient system performance and allows to reduce the impact of transient effects in optical multiband networks. Using feedforward control, relevant parameters such as pump powers and setting of the variable optical attenuator are derived from total power levels detected at the input of the amplifiers. For this purpose, either look-up tables or mathematical equations might be used.

A set of equations suitable for determining the gain and tilt settings of the amplifiers for various input conditions has been derived and their applicability has been verified by means of simulations. In the next step, the performance achievable with this technique shall be determined in an experimental setup. Therefore, a setup comprising two parallel amplifiers (C-band and L-band) has been created and the feedforward control is currently implemented. In a further step, an S-band amplifier shall be added to the setup.

Verification of the feedforward control for operation of a C-band and L-band system is targeted to finish end of January 2024. Integration of the S-band amplifiers (without control) is scheduled for March 2024.

3.3.2 Raman amplification

Hybrid erbium-doped fiber (EDF)/Raman amplifiers (HFAs) can be utilized to improve the performance of specific fiber spans in dense wavelength division multiplexing (DWDM) networks, aiming to extend the reach and/or increase the capacity of optical channels, thereby reducing the total number of line interfaces required to satisfy a given set of traffic demands. However, HFAs are costlier than simpler EDF amplifiers (EDFAs) since they include Raman pumps in addition to an EDFA. Consequently, it is paramount to place them only at selected fiber spans of the network to maximize their impact while keeping their number limited. It has been shown that HFA placement can be a complex task in mesh DWDM networks in view of optical channel diversity, with each fiber span traversed by multiple channels with different source and destination nodes. Multiband transmission will further increase the complexity of the HFA placement problem.

Ideally, the optimized placement of HFAs in a mesh DWDM network to minimize CAPEX would balance the savings in line interfaces (e.g., for 3R regeneration) with the additional cost of hybrid amplifiers. A global optimization problem consists of simultaneously optimizing the HFA placement and the routing of traffic demands, including channel format selection and spectrum assignment. However, it is well-known that even the standalone routing and spectrum assignment problem is already NP-hard. Jointly solving it with the HFA placement problem will result in an even more complex problem that could only be solved in very small instances. In fact, practical transport network design usually assumes that the optimization of the optical line system is loosely coupled with routing of traffic requests, that is, the line system (e.g., type of amplifiers, amplifier settings) is optimized first and either without information regarding traffic demands or by exploiting limited information, such as the paths that are expected to be more important to route traffic. Moreover, in cases where the traffic demands are unknown at the network planning stage and will be dynamically provisioned, e.g., via a SDN controller, the optical line system must be designed having in mind generic and network-wide reach metrics, such as the number of feasible optical channels between all or a sub-set of node pairs.

A practical approach to optimizing HFA placement is to prioritize the minimization of the number of (probable) 3R regenerators required over that of the number of HFAs. This corresponds to determining the maximal set of feasible optical channels, given full mesh connectivity or a sub-set of node pairs, followed by placing a minimum number of HFAs that ensure all channels in that set are feasible. The rationale behind this strategy is based on: (i) the fact that a single HFA improves the performance of all channels traversing that fiber span (e.g., up to 96 channels in C-band using a 50 GHz grid, approximately twice that number when also exploiting the L-band); and (ii) the evidence that in most DWDM network deployments the total cost with line interfaces (at the demand’s end nodes and as 3R regenerators at intermediate nodes) is significantly higher than that with optical amplifiers.

Building on the approximation that noise adds up incoherently along the transmission path, we have proposed optimal methods to solve the problem of placing hybrid amplifiers in mesh networks. Particularly, two integer linear programming models, one to determine the minimum number and location of HFAs required to reach a target set of feasible optical channels (i.e., without intermediate 3R regenerators) and another to maximize the number of feasible optical

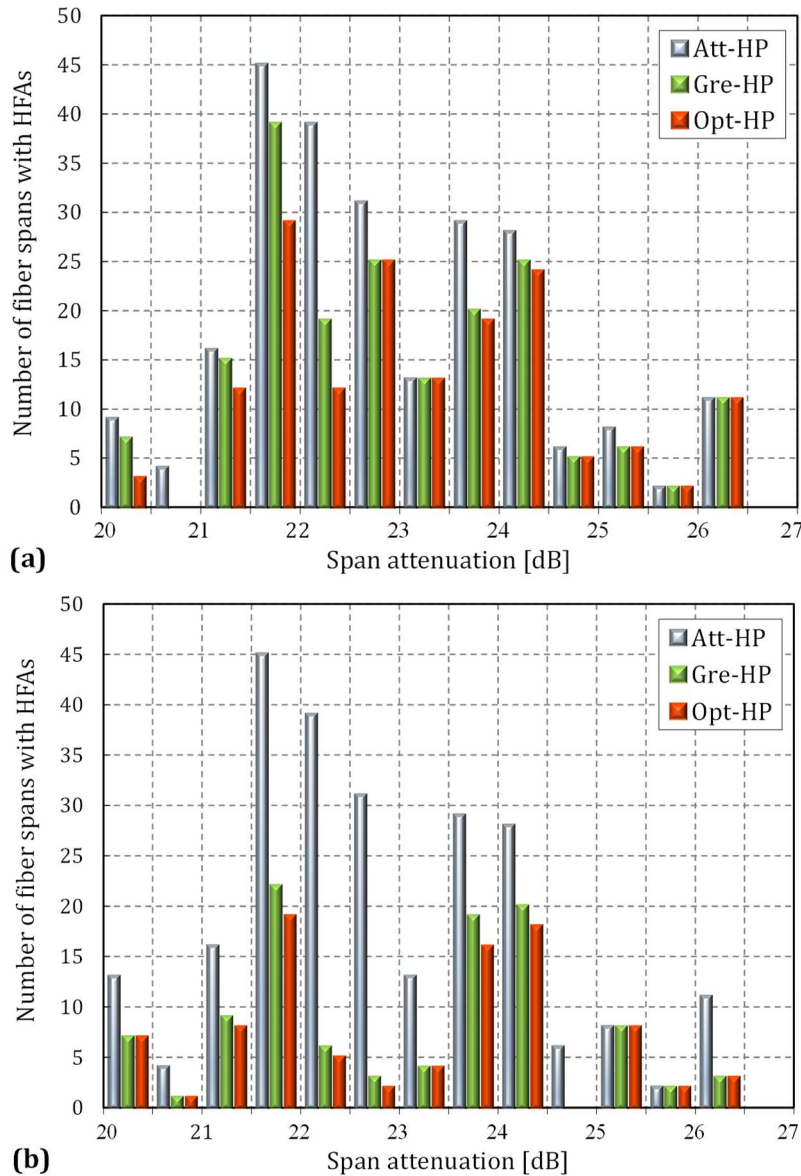


Figure 3-14 HFA distribution as a function of the fiber span attenuation for 20 dB and channel formats (a) 100G (QPSK) and (b) 200G (16QAM).

channels given a limited number of HFAs to be deployed, have been proposed (for details, please see [JOCNPedro]).

To illustrate the impact of the Raman placement approach, Figure 3-14 illustrates the HFA distribution for 3 placement strategies in a 49-node Pan-European network considering a C-band transmission system only. The placement strategy using an ILP model is denoted as Opt-HP, whereas Gre-HP consists in using a greedy heuristic algorithm and Att-HP is a simple

attenuation-based placement strategy. Further details on each of these approaches can be found in [JOCNPedro]. The results shown correspond to utilizing the optical channel formats 100G (QPSK) in Figure 3-14 (a), and 200G (16QAM) in Figure 3-14 (b). The plot for 100G shows that the largest share of savings from using Gre-HP or Opt-HP, versus Att-HP, occurs for span attenuations between 21.5 and 22.5 dB and between 23.5 and 24 dB. Moreover, the extra HFA savings from exploiting Opt-HP instead of Gre-HP are more pronounced in the former span attenuation interval. In the case of 200G, most HFA savings from using Gre-HP or Opt-HP are concentrated in the span attenuation range between 21.5 and 23 dB. Furthermore, the additional HFA savings from utilizing Opt-HP instead of Gre-HP are distributed over a wider range of span attenuation values.

Table 3-4 Number of HFAs as a function of the placement strategy for 3 channel formats.

Channel format	A_{min} (S')	$ T_{max} $	Number of HFAs, S*		
			Att-HP	Gre-HP	Opt-HP (†)
100G (QPSK)	25 dB (44)	1374	44	34	34 (0%)
	24 dB (112)	1592	112	108	108 (0%)
	23 dB (196)	1694	196	160	158 (-1%)
	22 dB (336)	1786	306	246	236 (-4%)
	21 dB (458)	1872	450	356	302 (-15%)
	20 dB (492)	1874	484	376	324 (-14%)
150G (8QAM)	25 dB (44)	550	44	32	32 (0%)
	24 dB (112)	664	110	90	88 (-2%)
	23 dB (196)	728	194	156	150 (-4%)
	22 dB (336)	750	306	234	214 (-9%)
	21 dB (458)	816	450	340	290 (-15%)
	20 dB (492)	820	476	352	298 (-15%)
200G (16QAM)	25 dB (44)	226	44	26	26 (0%)
	24 dB (112)	248	112	68	64 (-6%)
	23 dB (196)	262	178	114	104 (-9%)
	22 dB (336)	286	270	132	118 (-11%)
	21 dB (458)	310	450	188	166 (-12%)
	20 dB (492)	316	492	210	188 (-11%)

† difference versus best result with Att-HP and Gre-HP.

To quantify the impact of the HFA placement strategy, Table 3-4 illustrates the outcome of eighteen instances of the placement problem, when solved with three placement strategies. The number of unidirectional paths in this network when considering the shortest path is 2352. The eligible fiber spans to host a hybrid amplifier is given by $|S'|$, the size of the target set of feasible optical channels for each set of eligible fiber spans is given by $|T_{max}|$ and the set of eligible fiber spans hosting an HFA after using one of these placement strategies is denoted as S^* . Six different sets of eligible fiber spans were considered by varying the minimum span attenuation, A_{min} , from 20 to 26 dB, for a total number of eligible fiber spans between 44 and 492. This set of results provides insight into several aspects. Firstly, employing the simpler attenuation-based HFA placement strategy is ineffective. In six out of eighteen instances, no HFA savings are achieved, and in the remaining twelve the average savings, when compared to deploying HFAs at every eligible span, are 5%. As referred, this is a consequence of placing these amplifiers solely based on fiber span attenuation and not estimating how the performance improvement in certain fiber spans relates to the feasibility of specific optical channels. Secondly, adopting Gre-HP instead of Att-HP results in substantial savings in HFA count. The savings range between 4% and 58%, being 30% on average, and tend to be (i) larger when the number of eligible fiber spans increases (i.e., A_{min} decreases); and (ii) slightly larger when higher order

modulation formats are utilized. The higher number of eligible spans means a larger set of feasible optical channels, which results in more paths overlapping per eligible span. On the other hand, the use of higher order modulation formats translates to shorter feasible optical channels, which can make certain spans significantly more important than others to reach the target set of feasible optical channels. Both cases further stress the importance of deciding on the eligible spans to be upgraded with HFAs based on information of how many and which optical channels can be impacted. Thirdly, the results provide evidence of the superior performance of Opt-HP compared to that of Gre-HP. The former strategy provides extra HFA savings in most instances of the problem, with more expressive benefits when the number of eligible fiber spans increases. These larger HFA savings are attributed to the fact that, as the performance of each eligible fiber span potentially impacts a larger number of optical channels from the target set, the optimization problem becomes more complex, favoring the adoption of a strategy that guarantees finding the global minimum. In this network, the extra savings from using the ILP model reach up to 15%. Although the illustrative results presented in this section only consider C-band transmission, the proposed methodology can be used to evaluate the optimal placement of HFA in a multiband transmission systems as well.

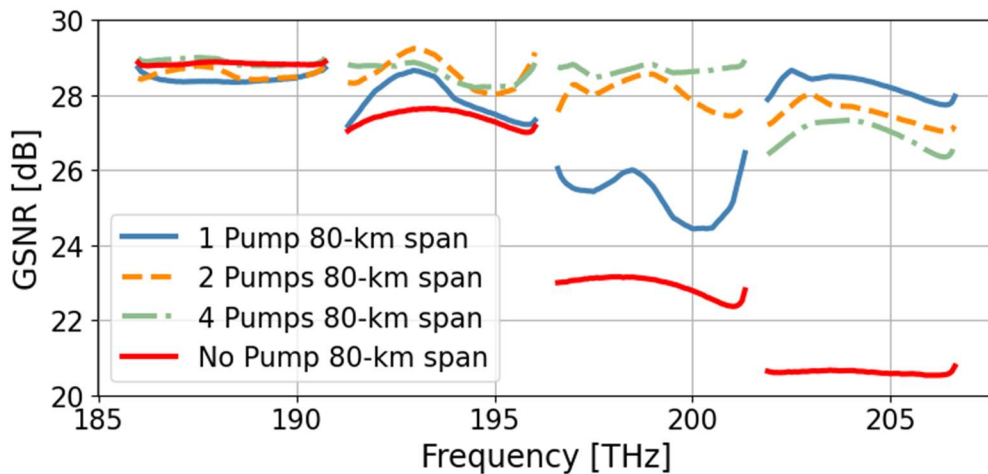


Figure 3-15 Illustration of the GSNR improvement in a multiband transmission system resulting from using HFA amplification in an 80km long SSMF span.

To better illustrate the impact of the Raman amplification in multiband transmission systems and stress why placing Raman pumps in such systems may be important, Figure 3-15 illustrates the potential GSNR improvement in an 80km long SSMF span of a C+L+S-multiband transmission system when deploying different number of Raman pumps. The analysis of Figure 3-15 shows that Raman amplification enables achieving similar GSNR in all transmission bands which potentially simplifies network planning and operation. Moreover, the optical performance in S-band is significantly enhanced by Raman amplification.

3.4 FILTERLESS SOLUTIONS

3.4.1 Performance analysis of metro-aggregation network scenarios

The exploration of coherent transmission within the metro-aggregation domain of the fibre networks has driven our analysis to focus on traffic aggregation as a strategy to address the growing traffic demands of this sector. Previously, our analyses highlighted solely the traffic aggregation aspect of relying on a PtMP transmission paradigm in metro networks, comparing the design and deployment considerations against traditional point-to-point systems

[JOCNBaeck]. The work has now been expanded to consider the impact of the evolution of traffic (i.e., growth) on the optical performance and the sharing of resources at the edge node sites, which has direct impact on the provisioning of the optical links.

Whereas in the first few analyses we focused our attention on two network topologies provided by Telecom Italia (TIM)— “urban-industrial” and “suburban-rural”—, we have since then built on our PtMP analysis by considering additional network topologies, as well as hardware optimization and sublink aggregation. The former relates to the positioning of amplifiers within the network topology to maximize their impact in terms of performance. The latter, on the other hand, refers to a metric that quantifies the degree of resource sharing at the edge nodes within a network [JOCNCastro]. By defining a performance threshold for the expected OSNR margin of the network, based on the simulated data, we can determine what would be the necessary hardware requirements to fulfil the desired performance level for a particular network. In this context, OSNR margin refers to the OSNR difference between the calculated descriptive OSNR level of a given network and the minimum OSNR level required for the channel coding of a PtMP coherent pluggable to operate effectively.

For example, in [JOCNCastro], for the “urban-industrial” scenario, where traffic flows in the direction of the edge node labelled ‘B’, Figure3-16(b) shows the transmission performance across the network depending on the number of EDFAs and the level

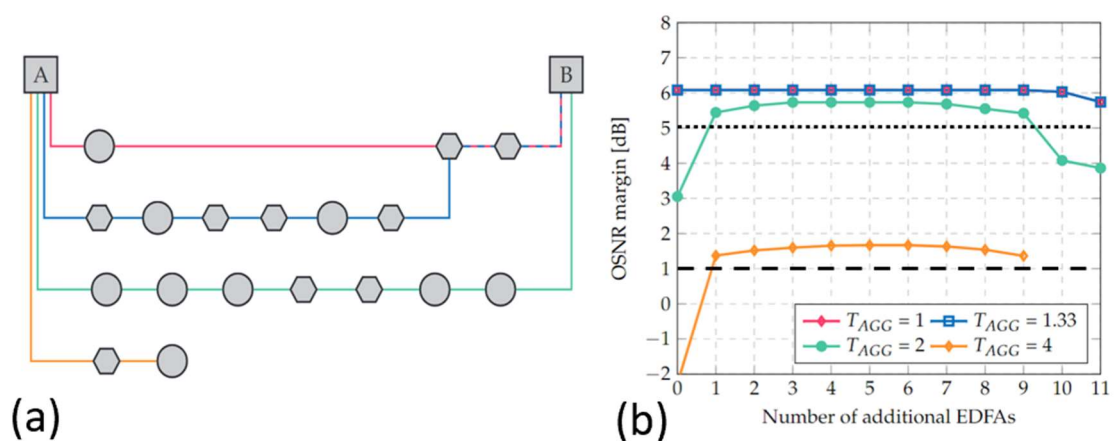


Figure 3-16. (a) Network topology for the “urban-industrial scenarios”, where each sublink (i.e., horseshoe) is depicted using a different colour for ease of visualization. Squares, circles, and hexagons represent edge nodes, leaf nodes, and transit nodes, respectively. (b) Transmission performance of (a) as a function of the number of EDFAs in the network and the level of sublink aggregation (TAGG). The dotted and dashed lines represent possible performance thresholds that could be used to determine the deployment conditions for a network.

of sublink aggregation, a metric represented by T_{AGG} . A higher value of T_{AGG} indicates that more horseshoes connect to the same high-speed PtMP pluggable at the edge node, whereas a value of 1 (i.e., the lowest possible value) implies that each sublink is being exclusively served by a single high-speed PtMP pluggable transceiver. In the case of the network topology in Figure 3-16(a), there are four possible levels, which are summarized in Table 3-5.

Table 3-5 Correspondence between T_{AGG} and the number of high-speed PtMP pluggables required at the edge node for the network topology shown in Figure 3-16 (a).

T_{AGG}	Pluggables at edge node
1	4 high-speed pluggables
1.33	3 high-speed pluggables
2	2 high-speed pluggables
4	1 high-speed pluggable

With the results shown in Figure 3-16(b), we can determine what kind of network implementation (i.e., in terms of margin, number of amplifiers, and/or number of high-speed pluggables) is realisable. Nevertheless, to do this, operators would need to define a minimum accepted performance margin; in other words, a minimum required OSNR that would ensure the correct and robust operability of a network that ensured a certain quality of transmission (QoT). In this scenario, for example, if an operator were to require a margin of 5 dB to deploy a network (represented by the dotted line in Figure 3-16(b), it is only possible to guarantee it when operating with T_{AGG} of 1, 1.33, and 2. A T_{AGG} of 2, however, can only meet the required margin in this case with at least 1 additional EDFA. If, by contrast, the required margin is lowered to 1 dB, now even a T_{AGG} of 4 is a valid realization for the network deployment; this would still require introducing at least 1 additional EDFA. With these realisations, it is evident how these considerations directly tie to the deployment and bill of materials, and here is where cost models come into play, since the question to be addressed becomes whether the reduction in one set of elements compensate the introduction of additional ones of a different kind (e.g., high-speed PtMP and amplifiers).

In [IMOCNelson], we delved further into detail regarding the transmission performance implications and characteristics of one of TIM’s network topologies as the reference network in D2.1. The network diagram is depicted in Figure 3-17: two edge nodes, where one serves as a protection, are connected via two horseshoes that share one transit node. This topology, contrary to the one in Figure 3-16(a) only has two possible levels of sublink aggregation: 1 and 2; or 1 high-speed PtMP pluggable for each link and 1 high-speed PtMP pluggable for both, respectively.

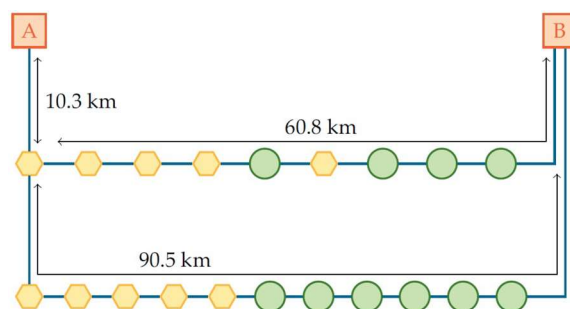


Figure 3-17 Network topology for the scenario analysed in [IMOCNelson]. Squares, circles, and hexagons represent edge nodes, leaf nodes, and transit nodes, respectively.

The performance analysis of this network focuses on exemplifying the trade-offs that occur when we focus on different aspects, such as the number of deployed EDFAs, T_{AGG} , the OSNR margin, and the launch power of the optical signal. In this regard, the results in Figure 3-17 offer us a glimpse into the characteristics of the network.

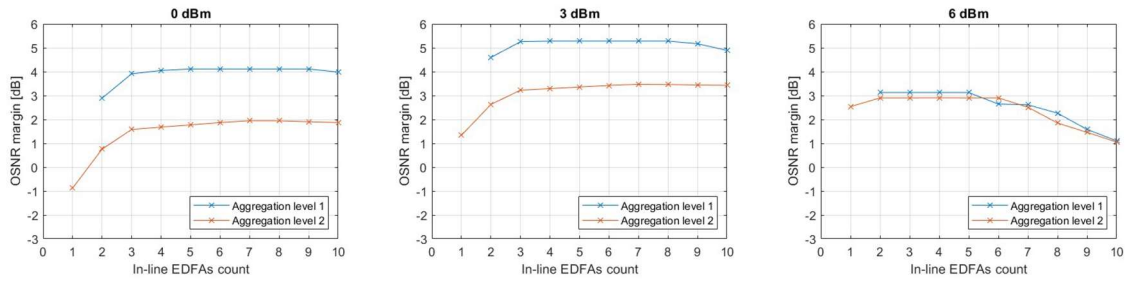


Figure 3-18 Transmission performance of Fig. 3-17 as a function of the number of deployed EDFAs in the network and the level of sublink aggregation as a function of the launch power of the optical signal. This scenario depicts traffic flowing in the direction of edge node ‘B’.

The first aspect to observe is the fact that due to the large number of transit nodes –nodes where there are no amplifiers by default—at the beginning of the horseshoes, the complete network needs a minimum of 2 amplifiers for the $T_{AGG} = 1$ case, one for each sublink, to overcome the losses at the beginning of the link. On the other hand, by aggregating the sublinks ($T_{AGG} = 2$), a single EDFA enables a successful transmission in this scenario. Nevertheless, this is not possible for a launch power of 0 dBm; for this to be the case, the launch power must be further increased to 3 dBm or 6 dBm depending on the desired margin threshold.

3.4.2 OADM FILTERLESS SOLUTIONS

To prepare for the demonstrators that are contemplated within the duration of the project, we have extended the framework of the simulation. The demonstrator, which is a collaborative effort from BT, TuE, and Infinera, has been upgraded in multiple aspects compared to the tool used before. First, the types of networks it can address has been expanded, allowing us larger degrees of flexibility regarding possible network topologies and scenarios, including. Furthermore, polarization-dependent loss (PDL) as a transmission impairment that translates into an OSNR penalty has been integrated into the simulator, where PDL is introduced amplifiers and couplers. Whereas previously non-linear impairments were also considered, the amount of penalty they would introduce was based on a signal with 16 DSCs; now, the simulator more accurately reflects the effects of non-linearities by determining OSNR penalties based on the number of subcarriers.

With the aforementioned upgrades, the discussion shifted towards the filter-less architecture that we had been investigating and how these nodes permit delivering and collecting the traffic to and from the leaf nodes (i.e., filter-less add/drop multiplexers) in a simpler and cost-effective way, which is of interest to operators because it makes upgrading and migrating towards higher-capacity technologies much easier. By using these optical add/drop multiplexers (OADMs), we also benefit from the flexibility of adding additional optical elements at the access nodes, which allow us to implement an optical continuum across access and metro-aggregation networks.

For this reason, BT, TuE and Infinera have been designing a filter-less OADM that will be used for the upcoming demonstration in BT-labs. With the components for the OADMs and their corresponding characterizations coming from TuE, Infinera and BT have further discussed the scenario for the demonstrator, where the focus lies on the P2MP XR optics technology in combination with the OADMs at the leaf nodes to enable metro-aggregation.

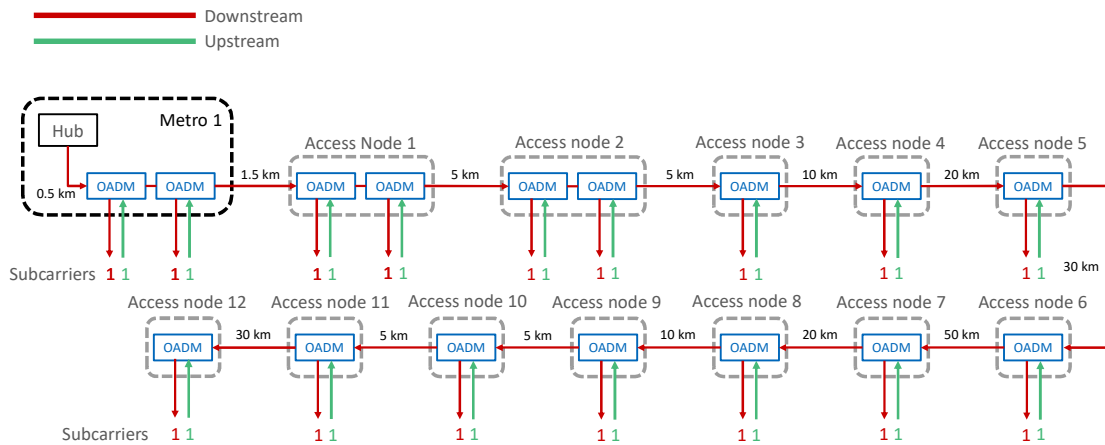


Figure 3-19 High-level schematic network diagram for the demonstrator at BT-labs.

For preliminary simulations of the demonstrator, as illustrated Figure 3-19, we are considering an optical transmission line, where a high-speed 400 Gb/s PtMP coherent pluggable transceiver powered by digital subcarrier multiplexing (DSCM) communicates simultaneously with multiple traffic aggregation nodes (i.e., OADMs). Since the precise architecture of the OADMs will be explained in detail in a subsequent section of this document, for now it suffices to say that each OADM stage refers to a PIC—a design lead and manufactured by TuE—which comprises add/drop couplers and SOAs. The transmission line consists of 16 OADMs, which are separated by fibre spans of different lengths (see Figure 3-19). To ensure the success of the demonstrator, the OSNR performance margins based on the SOA characteristics are being investigated by Infinera, who are leading the development of the simulator and carrying system-level simulations. Therefore, it was important to have an accurate model of the SOA, which was built thanks to extensive characterization measurements from TuE. Figure 3-20 shows the thoroughly measured gain and noise figure of the SOA at a wavelength of 1556.56 nm. In addition, TuE has provided the expected PDL of the SOA also as a function of the input power and current of the amplifier. This allows the simulator to mirror the actual operating point of the amplifier based on the scenario (e.g., downstream, or upstream) to calculate the performance of the link more accurately. Finally, as mentioned, non-linearities are considered in as much as the corresponding OSNR penalty is drawn depending on the launch power of the subcarriers and the number of subcarriers present in the optical signal.

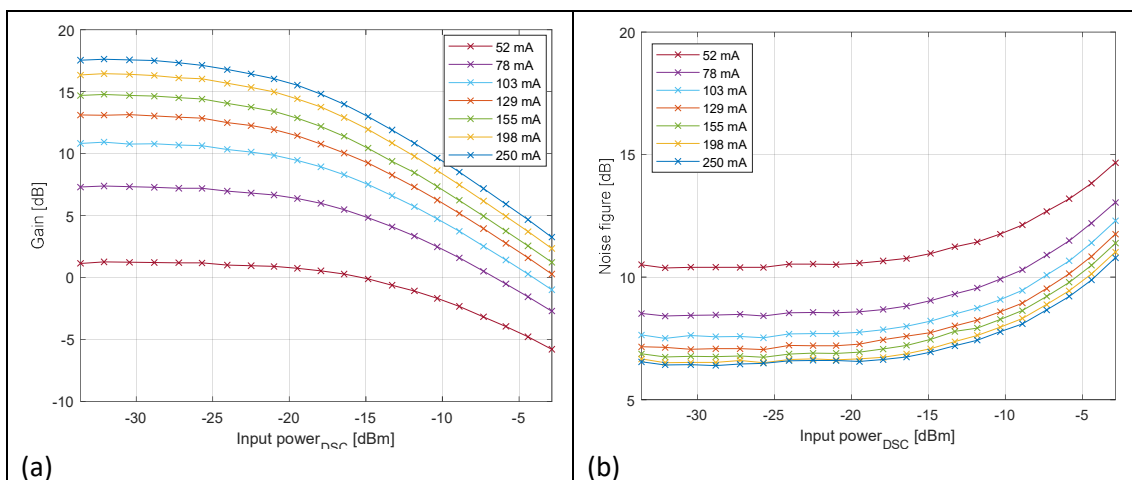


Figure 3-20 (a) Gain of the SOA as a function of the input power per subcarrier and the current of the amplifier. (b) Noise figure of the SOA as a function of the input power per subcarrier and the current of the amplifier.

At the moment, this work is just starting and will require a further upgrade of our evaluation tools. This will, however, enable the thorough evaluation of the network topologies in [JOCNCastro], allowing us to better estimate the usage and optimization of resources across the network, and how it influences the system performance.

3.4.3 Filter-less OADM upgrade strategies

The initial design of the filter-less OADM that will be used in the demo to be built in BT labs, as part of WP5 has a very simple configuration using 3 or 4 SOAs, and two optical taps (i.e., splitters with different coupling ratios), which is shown in Figure 3-21

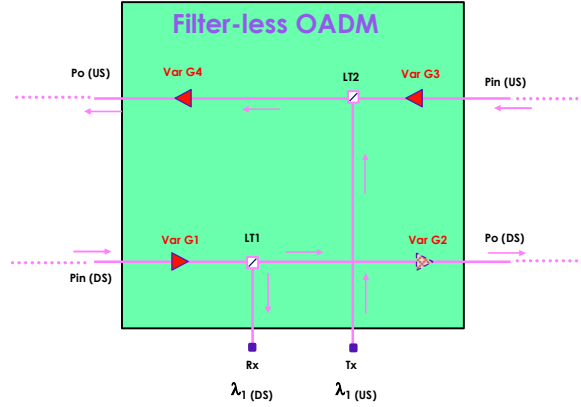


Figure 3-21 Initial Filter-less OADM configuration with 3 or 4 SOAs and 2 optical taps

This OADM design fits in a metro-aggregation network as described in the previous subsection, and subsections 2.1 & 2.6. It can be used to add/drop traffic from/to an XR optics Leaf in the access node, which will be connected to an XR optics Hub located in the metro node. The SOAs have a variable gain, which will be controlled by the B5G-ONS, such that the connection at the physical layer between the hub and the Leaf is attained. The SOAs in the downstream (or downlink) direction are used to overcome the losses of the transmission fibre and the optical tap, hence, depending on the fibre distances between OADMs, one or two SOAs will be needed. In the upstream (or uplink) direction, however, the first SOA, along with the transmitted power at the Leaf, are used to equalise the optical powers between the incoming DSC multiplex and the added DSC from the local Leaf. The second SOA in the upstream direction is used to overcome the transmission and tap losses.

The equation that gives the necessary gain of the equalisation SOA is:

$$G_3 = P_a - P_{in}(US) + 10 \log(n_i) - 10 \log(n_a) + LT2_t - LT2_a \quad (3 - 2)$$

And the necessary gain of the second SOA is given by:

$$G_4 = P_0(US) - 10 \log \left(10^{\frac{P_{in}(US) + G_3 - LT2_t}{10}} + 10^{\frac{P_a - LT2_a}{10}} \right) \quad (3 - 3)$$

Where

Table 3-6 Parameters

Param.	Description
G_3	gain of SOA 3 (dB) at the input of the U/S path
G_4	gain of SOA 4 (dB) at the output of the U/S path
Pin (US)	total optical power input (dBm)
n_i	number of DSC input
Pa	total optical power added (dBm)
n_a	number of DSC added
LT2t	LT2 insertion losses Through path (dB)
LT2a	LT2 insertion losses Add path (dB)
Po (US)	total optical power output (dBm)

It is important to investigate the possible methods to upgrade the filter-less OADM node when used along the Open XR system. There are 2 reasons we may need to upgrade the initial design:

- a) Upgrade the number of Leafs in the access node
- b) Upgrade the capacity of the metro-aggregation optical system.

If we want to upgrade the number of Leafs in the access node, there exist two possibilities:

- a.1) Use back-to-back initial OADM design (current option)
- a.2) Use an external optical splitter (50% ratio) connected to the initial OADM design

If we need to upgrade the system capacity, we have three options:

- b.1) Upgrade the XR optics to 800G
- b.2) Add a second 400G XR at a different wavelength
 - b.2.1) using back-to-back initial OADM design
 - b.2.2) adding an external splitter to the initial OADM design

These options will be analysed and evaluated in the coming months and reported in the future deliverable report D3.3.

3.4.4 (SEMI-)FILTER-LESS ADD/DROP NODE PROTOTYPE

Within the scope of B5G-OPEN a multiband (semi-) filter-less add/drop node prototype is designed to prepare future networks for multiband scalability. The prototype enables selected band bypass and add/drop capabilities for the S-, C- and L-bands as shown in Figure 3-22. This cost-effective structure is composed of four multiband multiplexers (MB Mux and MB Demux) and an optical matrix switch responsible for routing the bands accordingly. Monitor couplers are

also introduced at the input and output for effective monitoring of the ports during validation and operation of the prototype. The switch is fully programmable, allowing for remote operations between the multiple inputs and outputs.

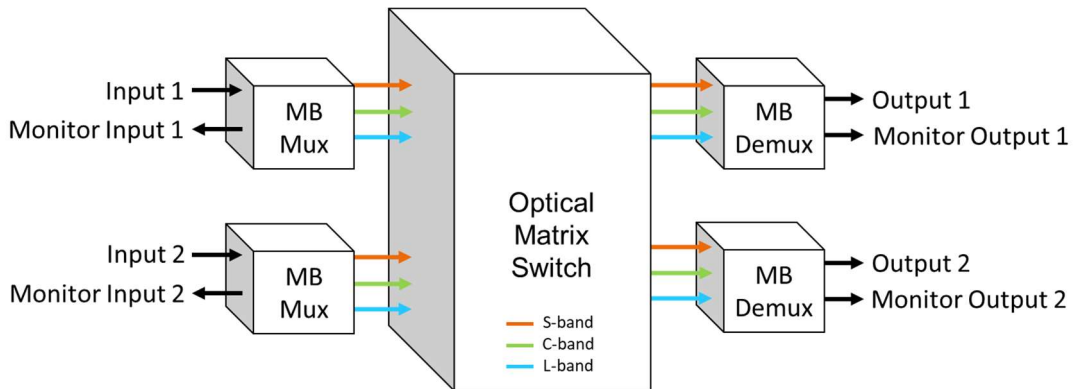


Figure 3-22 Architecture of (semi-) filter-less add/drop node, enabling whole-band operations.

After assembly, the prototype was characterized using a polarization-dependent loss analyzer (PDLA) to verify insertion loss (IL) and PDL of the multiple paths. The assembled prototype and the characterization curves can be observed in Figure 3-23, where it is possible to note an average IL below 3 dB and a PDL below 0.1 dB across all bands for all pathing possibilities of the prototype. These values are also presented in Table 3-7, where the specifications of the device are summarized. The gaps observed in the transitions of the bands occur due to the overlap of the distinct transfer functions of the band-specific filters that compose the MB Mux and MB Demux. Thus, these transitional regions are out of the specification of MB of operation of the device.

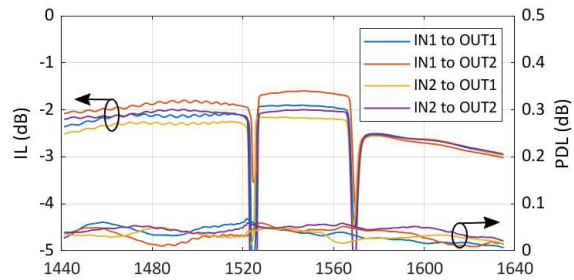


Figure 3-23: Prototype assembled at HHI's laboratory (left); and PDLA characterization of the prototype's input and output routing options for IL and PDL parameters (right).

Table 3-7 Prototype specifications.

Parameter	Specification
Operation Bands	S-band: 1460-1522 nm C-band: 1527-1565 nm L-band: 1574-1640 nm
Insertion Loss	< 3.0 dB
PDL	< 0.1 dB

As a proof of concept, two distinct MB signals were introduced to the device, one at each input as shown in Figure 3-23. The 50 GHz ASE dummy channels were generated using a combination of band-specific WSS and noise sources. A total of 125 channels compose the S-band, 92 compose the C-band and 90 for the L-band. All ports are monitored through 20-dB couplers contained in the prototype for monitoring purposes as shown in Figure 3-23, thus the measurements present a lower power spectral density than what is expected at the actual input and output ports. In Figure 3-23 (a), the signals of each input are forwarded to the corresponding output, however, in Figure 3-23 (b) the signals are routed to the opposing ports (all bands at input 1 are forwarded to output 2 and all bands at input 2 are forwarded to output 1), showing the fibre switching capability of the device.

Another experiment demonstrates the add/drop capabilities of the device in terms of whole-band operations. Figure 3-24(a) demonstrates the outputs of the device when the whole C-band is dropped from input 1 and when the whole L-band is dropped from input 2. Figure 3-24(b) showcases a more complex operation, where the S-band from input 1 is forwarded to output 2 and the C- and S-bands are dropped completely. As for input 2, the L- and C- bands are forwarded to input 1, while the S-band is routed to output 2. This demonstrates the multiple complex whole-band operations that are made possible by the device, thus validating the prototype for its intended purposes within the project.

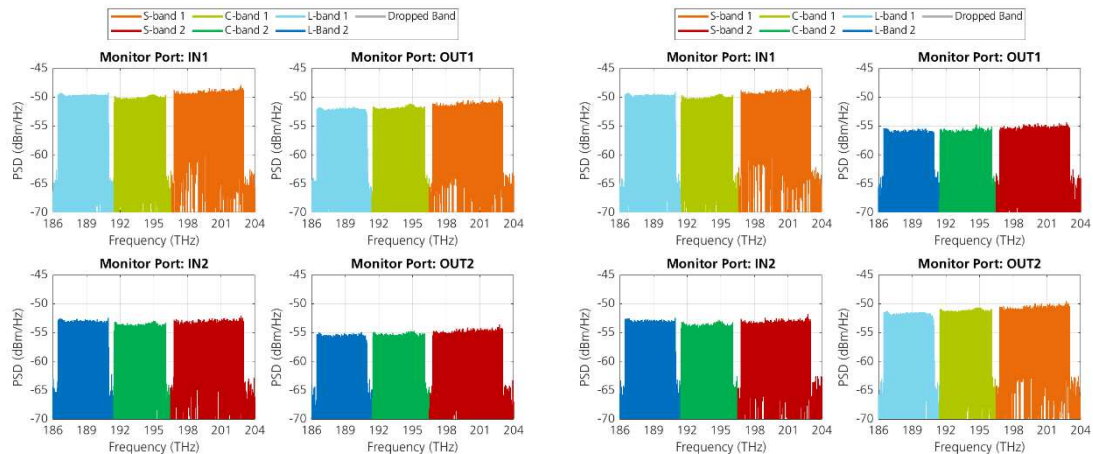


Figure 3-23(a) MB signals at input 1 and 2 being forwarded to the corresponding output ports 1 and 2; and (b) demonstrating the fibre switching capability of the device.

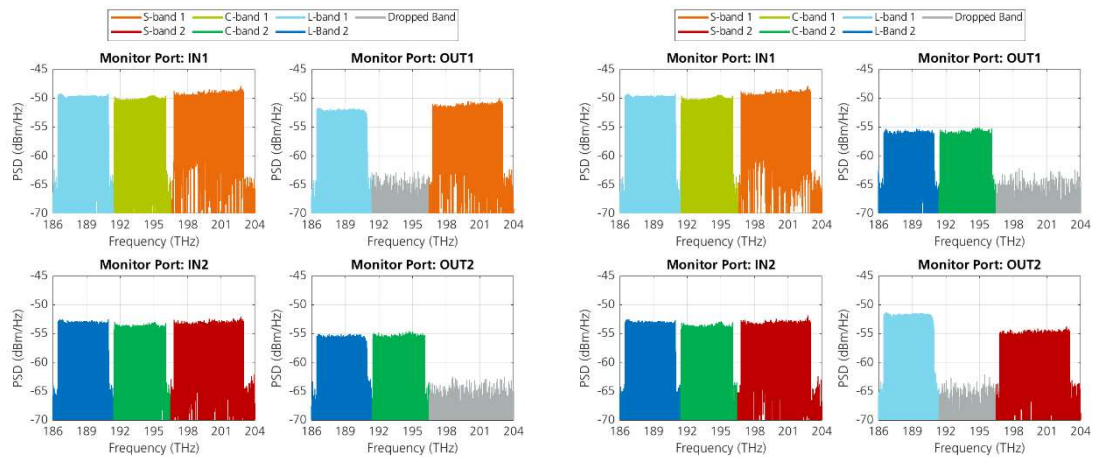


Figure 3-245: (a) C-band of input 1 and S-band of input 2 being dropped; and (b) multiple whole-band add/drop operations between the ports.

4 INTEGRATED ACCESS AND X-HAUL OPTIONS

4.1 B5G-OPEN ACCESS NETWORK ARCHITECTURE

One of the key features of B5G-OPEN is the Integrated Access where any access technology system is seamlessly operated and controlled [D2.1].

Access CO architectures were described in Section 4 of D2.1 distinguishing along time frames, and in Section 2.6 of this report the optical node has been dimensioned. Also in D2.1, different access technologies are mapped onto the B5G-OPEN access COs architectures.

In this section, a very brief summary of a tool to plan services across the B5G-OPEN network is presented (a full tool presentation is given in WP4 deliverable D4.2), and next a detail description of LiFi is also presented.

4.2 AN ACCESS PLANNING TOOL

The B5G-ONP component is a control plane module, further presented in Section 5 of D4.2, that facilitates the coordination and orchestration of IT and network resources. This module offers a range of capabilities, including the provisioning of tools for designing, optimizing, and planning the deployment, administration, and configuration of services and resources within the network infrastructure.

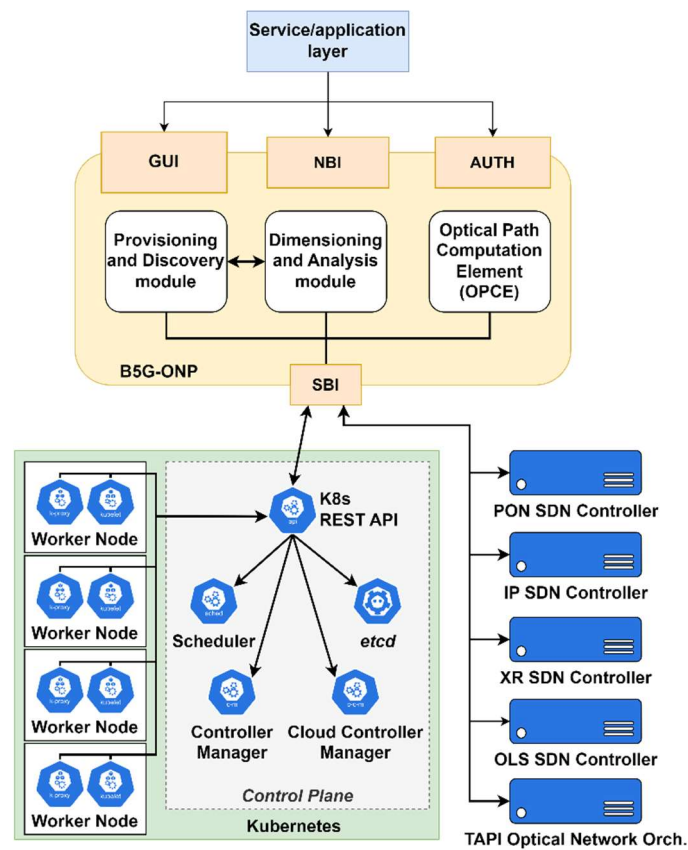


Figure 4-1: Architecture and interconnection of B5G-ONP component presented in D4.2

The B5G-ONP component operates as an integrated unit, incorporating various modules to enhance network performance while meeting global requirements. As depicted in Figure 4-1, these modules include:

- **Provisioning and Discovery Module:** This module automates the allocation of physical and virtual network resources, aligning with user requests and policies. It scans and imports network topologies, identifies services and dependencies, and centralizes this data for efficient network management.
- **Dimensioning and Analysis Module:** Responsible for forecasting and optimizing network performance, this module employs data analytics and machine learning to analyze traffic patterns and resource utilization. It predicts network performance needs, including capacity, latency, and jitter, aligning them with network topology and application requirements.
- **Optical Path Computation Element:** This module evaluates technical variables to determine the optimal optical connections route. It minimizes congestion and enhances efficiency by estimating the performance of potential paths and configuring resources, such as the Optical SDN Controller, to ensure Quality of Transmission (QoT).

Thus, according to D4.2, the interfaces involving the B5G-ONP can be categorized into three main types:

- **B5G-ONP – Service/Application Layer Interface:** This interface provides verticals and service/application layer consumers with both a graphical interface and an Open NBI

API. It enables the orchestration of network services, applications, network slices, or DSR and IP flows. For more details, refer to Section 4.11 of D4.2.

- *B5G-ONP – Kubernetes Interface*: From a client-side perspective, the B5G-ONP utilizes the default Kubernetes API. Firstly, it retrieves essential IT and deployment metrics to gain cluster visibility for deployment recommendations. Secondly, it commands Kubernetes for network application provisioning using available computational resources in the Kubernetes cluster. Further information available in Section 4.12 of D4.2.
- *B5G-ONP – SDN Controllers Interface*: This interface encompasses communication between the B5G-ONP and various SDN controllers responsible for different network domains within the B5G-OPEN project, such as IP, PON, XR, or Optical domains. These interfaces focus on obtaining network topology-related metrics and instructing SDN controllers for network slice and connection provisioning. Different protocols and APIs are envisioned for communication with each controller type, as previously described in Section 4 of D4.2.

The status of the integration of B5G-ONP with the rest of the corresponding elements is on-track and some the interfaces and interactions are already tested and validated in WP5 demos and other related works. All the available details on B5G-ONP integration can be found in Section 5.4 of D4.2.

4.3 LIFI ACCESS

In this section, the implementation of the LiFi access prototypes is presented. It includes a set of devices that could convert and deliver data packets in the form of light. These devices are:

- LiFi AP.
 - A Physical layer implementation based on 802.11 OFDM PHY.
 - Digital-to-analogue and analogue-to-digital converters which convert the digital signal to analogue signal for downlink transmission, and convert the received analogue signal to digital signal for uplink decoding.
 - A MAC layer interface between the PHY and the upper layers, with functions defined in IEEE 802.11. The implemented MAC could be modified to provide full-duplex operation, high protocol efficiency and multiuser support.
- LiFi transmitters and transmitter drivers. The transmitters act as both luminaire for illumination and antenna for optical wireless signals. It is usually an LED lamp for general use cases, and it can be within either visible light spectrum or infrared spectrum. The transmitter drivers are the electronics which ensure the transmitters work in optimised conditions.
- LiFi user dongle, or a Station unit. It is the user device that receives downlink signals and sends uplink signals.

a) IEEE 802.11 OFDM PHY

According to OFDM PHY described in [IEEE802.11 OFDM PHY], the system provides a WLAN with data payload communication capabilities of up to 54 Mbps. The system uses 52 subcarriers that

are modulated using binary or quadrature phase shift keying (BPSK or QPSK) or using 16- or 64-quadrature amplitude modulation (16-QAM or 64-QAM). Forward error correction coding is used with a coding rate of 1/2, 2/3 or 3/4. Major parameters of the OFDM PHY are shown in Table x[IEEE802.11 OFDM PHY].

Table 4-1: Major parameters of the IEEE 802.11 OFDM PHY

Information data rate	6, 9, 12, 18, 24, 36, 48 and 54 Mbps (20 MHz channel spacing)
Modulation	BPSK OFDM, QPSK OFDM, 16-QAM OFDM, 64-QAM OFDM
Error correcting code	K=7 (64 states) convolutional code
Coding rate	1/2, 2/3, 3/4
Number of subcarriers	52
OFDM symbol duration	4.0 us
Occupied bandwidth	16.6 MHz

The standard format for the Physical layer protocol data unit (PPDU) is shown in Figure 4-2. The PHY Preamble field is used for synchronization. It consists of 10 short symbols and 2 long symbols. The PHY Preamble is followed by the SIGNAL field and DATA. The SIGNAL field contains information such as the type of modulation and the coding rate as used in the rest of the packet, and the length of the data to be transmitted. The DATA field includes the PHY service data unit (PSDU) with additional SERVICE field, tail and pad parts.

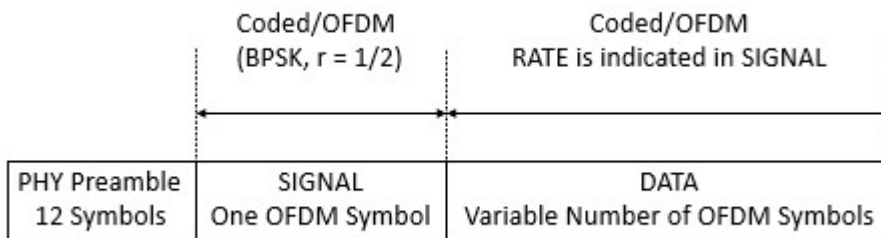


Figure 4-2 PPDU format

b) LiFi PHY

In LiFi, as light signals must be unipolar/positive and real, OFDM needs to be modified for being adapted to LiFi. DC biased optical OFDM (DCO-OFDM) is one method by adding a DC bias to ensure signal is unipolar. Also with a Hermitian symmetry arrangement, the signal is ensured to be real. In the LiFi prototype, the PHY is implemented based on IEEE 802.11 OFDM PHY with modifications which suits for LiFi applications. The architecture of the transceiver follows standard OFDM system design and the block diagram for both transmitters (Tx) and receiver (Rx) are shown in Figure 4-3

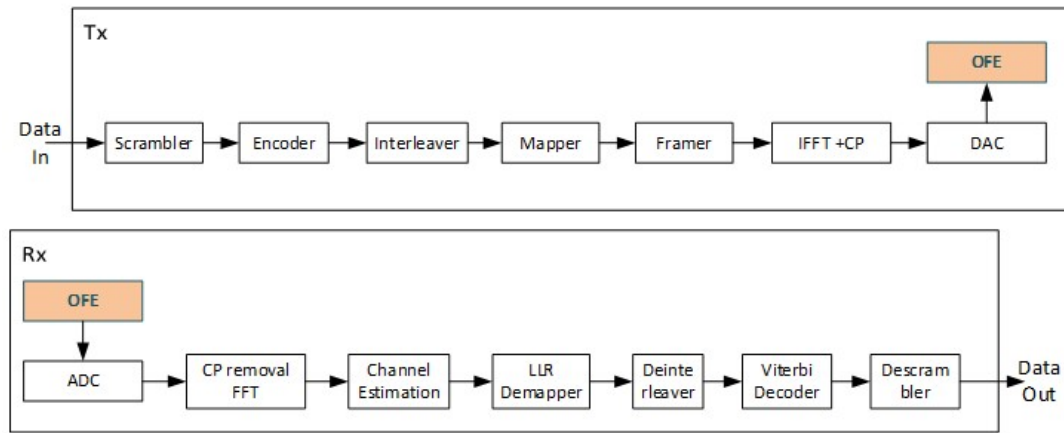


Figure 4-3: Block diagram of baseband Tx and Rx architectures.

c) LiFi MAC

The LiFi MAC is implemented based on the point coordination function defined in IEEE 802.11. Modifications have been made for the requirements of LiFi applications. The modified point coordination function protocol offers high protocol efficiency and multi-user support.

d) Optical front-end components

The downlink transmitter is commercial white LEDs which are made from blue LEDs at around 450 nm with a phosphor coating. As phosphor response is low which would limit the modulation bandwidth of LEDs, blue bandpass filters are used. In the uplink, IR LEDs at around 850 nm are used.

On the receiver end, it converts light into electrical current while the conversion efficacy is represented by the responsivity (in A/W). Avalanche photodiodes (APDs) are used due to their high gain in the signal amplification. Two stages of amplifier are used including a transimpedance amplifier (TIA) and the second-stage amplification. These amplifiers could enhance the signal output after the APDs.

5 PACKET AND OPTICAL MONITORING

5.1 LONGITUDINAL POWER PROFILE MONITORING

Recently, successful estimations of longitudinal power profiles were demonstrated from a single coherent receiver based on nonlinear back-propagation techniques [Tan20, Sas20, Tan21]. This allows a distance-wise monitoring of physical parameters.

In this deliverable, we propose other methods and extensions to the initial power profile technique introduced in [Tan19]. A first contribution focuses on the applicability of power profile technique to ultra-long transmission link. A second contribution is the introduction of a new technique to monitor an extra-loss or dispersion anomaly along an optical fiber baser on XPM analysis. Finally, we study the advantage in term of cost of relying on digital power profile monitoring technique rather than on OTDR for different networking topologies.

5.1.1 Longitudinal Power Monitoring over a deployed 10,000-km Link

We demonstrate the power profile estimation over a deployed 10,000-km submarine link using digital processing at the receiver with a correlation-based method and no chromatic pre-dispersion [May23].

The experimental set-up is described in Fig.5.1. We perform our experiments with a multi-channel transmission with two different spectrum allocations. The channels under test (CUT) are PDM-QPSK modulated at 69 Gbaud. They are shaped with a root-raised-cosine filter with 0.01 roll-off factor. Sequences of 2^{17} symbols are used for the transmitted signal.

No digital chromatic pre-dispersion is applied. For the transmitted bandwidth, we consider two configurations. For the 69-Gbaud case, we successively position the CUT at 56 different wavelengths ranging from 1534.25 to 1567.34 nm. The bandwidth is loaded with amplified spontaneous emission (ASE) channels to reach for 56 channels 75-GHz spaced. The channels are sent into a straight line of 56km-long Pure Silica Core Fiber spans with $110 \mu\text{m}^2$ effective area.

For the 69-Gbaud case, the line reaches 10,819-km. We amplified the signal using 4.2 THz-wide C-band EDFAs operated in constant output power mode at 16.5 dBm to approach a real submarine operating point configuration.

The input span launch power of each channel is therefore equal to -0.98 dBm, which is 0.5 dB below the nonlinear threshold. The CUT is then sent to an offline coherent receiver with 70 GHz

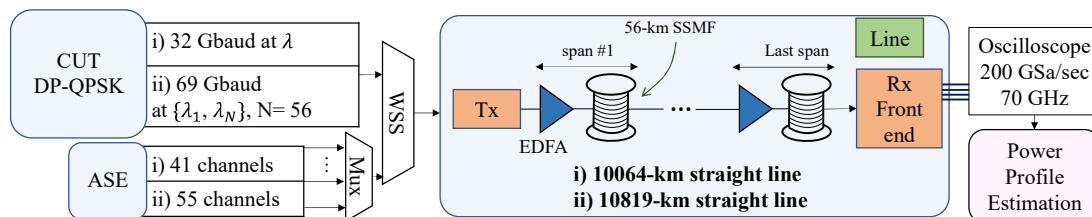


Figure 5-1: Experimental set-up. WSS: wavelength selective switch. Mux: multiplexer. SSMF: standard single mode fiber.

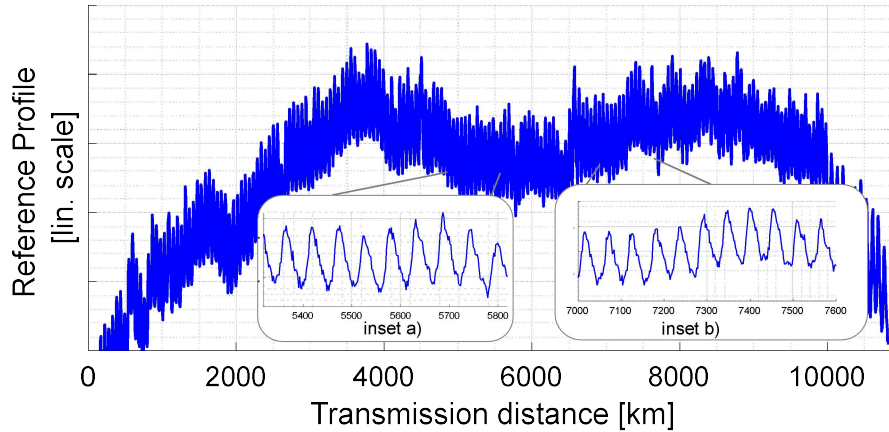


Figure 5-2: Experimental results. Power profile computed for the whole 10,819-km line at 69 Gbaud. Insets zoom the profile for [5320-5820]km (a) and [7000-7600]km (b)

bandwidth and 200 GSamples/s real-time oscilloscope and process offline. We record 2 acquisitions for each of the 56 channel frequencies leading to 112 acquisitions of 2.6×10^6 samples – at 2 samples per symbol (sps).

The power profiles were computed using the algorithm described in [Tan20]. To map the distance with the chromatic dispersion, we use the ratio of the accumulated value of the dispersion over the total distance to define the amount of CD to be compensated at each coordinate of the profile. However, this ratio is only an average value and adds uncertainty to the coordinates.

We plot in Fig.5.2 the power profile for 69 Gbaud through the whole link and in insets the zooms of the same power profile on restricted distance. The step chosen in Fig.5.2a) and Fig.5.2b) is 2 km, meaning for example that for the axis 7000-7600 km, 300 coordinates were computed. In Fig.5.2a) and Fig.5.2b), we see that the peaks are distributed periodically, which shows that the spans have the same length. To estimate the accuracy of the measured topology, we calculate, for 22 sets of 5 acquisitions, the distance for 10 spans for Fig.5.2.b) and then we average. We get a mean value of 54.9 km with a standard deviation of 0.49 km for the average span length over these 10 spans, which is close to the averaged span length of 55.3 km in this distance range. As the step used is 2 km and therefore the maximum accuracy is 0.2 km (i.e., step size/number of spans). To sum up, by leveraging the number of channels to compute power profiles, we can infer the topology of the 10,819-km link, here demonstrated on a subset of the link, fitting well the actual topology.

We are able to infer the topology and to monitor two 3dB power anomalies occurring simultaneously at 4,804 and 7,111km. This demonstration confirms the technique validity for troubleshooting in long optical connections, also suitable for submarine links.

5.1.2 Locating Fiber Loss Anomalies with a Receiver-side Monitoring Algorithm exploiting Cross-Phase Modulation

In the literature, edge-side monitoring techniques have been developed by exploiting the non-commutative interaction between Kerr and dispersive fiber effects through the capabilities offered by coherent detection. Of particular relevance are the fiber-longitudinal monitor methods based on back-propagation techniques [Tan20, Sas21] that provide a tomography of the optical link by scanning the coordinates one-by-one. However, such techniques require

many discrete Fourier transforms. A technique based on XPM was proposed in [Hui22], but it requires special sequences and operation during maintenance mode.

In this work, we exploit XPM between a supervisory channel (e.g., through a super-channel) and the CUT to detect the coordinate of loss anomalies with a resolution of a few km. The proposed method does not require high CUT powers, special Tx/Rx, nor an exhaustive anomaly search. It exploits the localized nature of nonlinear pulse collisions during propagation [Dar16].

Two channels propagating in an optical fiber interact through XPM. In the time domain, XPM is the result of collisions among pump channel pulses with probe channel (aka CUT) pulses. In general, four pulses collide, three coming from the nonlinear Kerr effect, and one from the matched filter impulse response [Dar16]. Such collisions are localized in specific link sections since the pulses travel at different speeds. Therefore, the interaction contains a signature of the local link's physical properties during the collision. To extract such information, we focus on two pulse collisions, which, under perturbative assumptions, induce only a phase distortion $\varphi_i = -\sum_k |b_k|^2 S_{i-k}$ on the detected i th CUT symbol [Dar16], where b_k are the known complex symbols of the interfering channel, modulating the pulse $p(z,t)$, with t time and z distance. Their nonlinear interaction is weighted by the discrete-time impulse response S_i :

$$S_i = \frac{8}{9} \gamma \int_0^{L_t} f(z) \int_{-\infty}^{\infty} |p(z, t + iT - \tau(z))|^2 |p(z, t)|^2 dt dz \quad (5-1)$$

with γ the fiber nonlinear coefficient, $f(z)$ the link power profile, L_t the link length. $\tau(z)$ is the channel walk-off that plays a fundamental role in localizing the collision, see Fig.5.3 (left) for a sketch. $p(z,t)$ is the pulse distorted by chromatic dispersion only. For instance, in typical fibers and with the assumption of sinc transmitted pulses, after a few tens of km $|p(z,t)|^2$ takes a rectangular shape in intensity [Dar16], of width linearly increasing with z . Although (5-1) has been introduced in scalar propagation, its generalization to dual polarization is straightforward [Dar16]. To localize the anomaly we monitor S_i . Since S_i relates φ_i and $|b_i|^2$ through a convolution, its minimum mean square error estimate is, according to Wiener filter theory, proportional to the covariance between φ_i and $|b_i|^2$, which can be efficiently estimated by averaging the convolution $(|b_i|^2 - \mathbb{E}[|b_i|^2]) \otimes (\varphi_i - \mathbb{E}[\varphi_i])$ with E expectation. The key point is that the time lags i are uniquely related to the starting/ending coordinate of the collision through the channel walk-off, hence, each i sample of S_i contains a localized signature of the link, and we can explore all coordinates at once performing the convolution. Some impairments affecting the estimation, such as amplified spontaneous emission (ASE), SPM, three-, and four-pulse collisions, are averaged to zero by collecting samples.

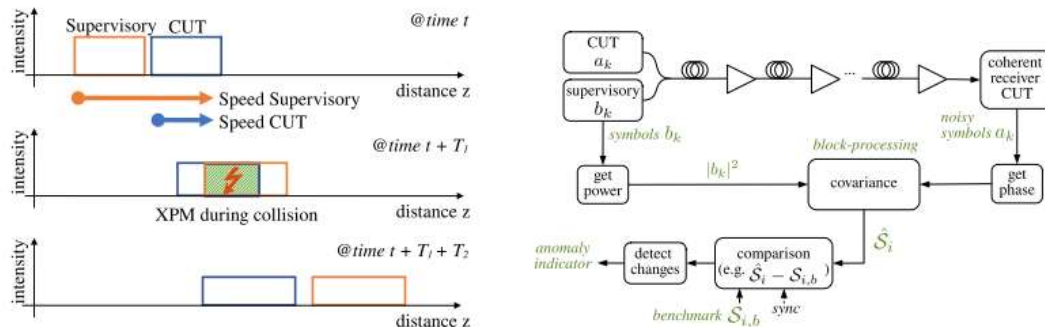


Figure 5-3: Left: example of two-pulse collision. Right: proposed algorithm for anomaly detection

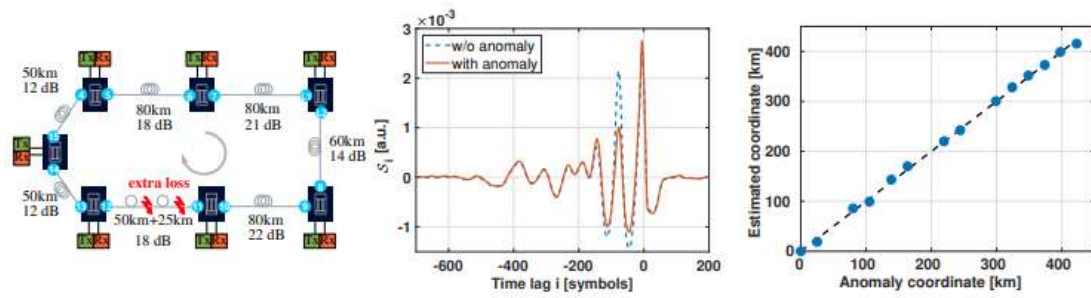


Figure 5-4: Experimental results. Left: setup. An extra loss is placed in correspondence with one red arrow. The Tx/Rx signals are injected/detected at a given ROADM. Center: phase impulse response given by the algorithm of Fig. 5.3 without anomaly (dashed) and with anomaly after 80 km (solid). Right: estimated anomaly coordinate.

We are thus looking for averaging time rather than complexity in chip area. Nevertheless, with data rates of the order of Gbd, the anomaly can be localized in seconds. Finally, by comparing S_i with a benchmark one an anomaly can be detected. The block diagram of the proposed algorithm is given in Fig.5-3 (right).

We experimentally investigated the proposed anomaly detector by using the 7-Nodes Optical Network testbed depicted in Fig. 5-4 (left). It describes a 470 km demo ring-network composed of seven nodes. Each node contained two optical amplifiers and a reconfigurable optical add-drop multiplexer (ROADM). The network was loaded with ASE channels. The CUT was a 33.6 Gbaud polarization-division multiplexed quadrature amplitude modulation (PDM-4QAM) channel generated by a commercial Nokia transponder (1830 PSI-2T). The supervisory channel was a 32 Gbaud PDM16QAM signal driven by a 216 pseudo-random sequence with a spacing of $\Delta f_{cs} = 200$ GHz to the CUT. We collected 670 M_{symbols} to better average out any non-two-pulse collision. Each channel had a power of 5 dBm and a pulse roll-off $\rho = 0.4$ (in numerical simulations we observed essentially no impact of ρ). The average fiber dispersion was 16.8 ps/nm/km, while the average fiber attenuation coefficient was 0.24 dB/km. We launched the CUT and the supervisory channel at the same node and detected the CUT after a round-trip. The anomaly was a 3 dB optical attenuator placed at the beginning or after 25 km of a given span, see the red arrows in Fig. 5.4 (left). We tested injecting the signals sequentially in all ROADM, which is equivalent to varying the anomaly coordinate along the link. We detected the CUT by a coherent receiver and a 200 Gsample/s real-time oscilloscope. Figure 5.4 (center) shows an example of S_i , smoothed over 50 taps, estimated with/without an anomaly at 80 km. S_i shows an oscillating profile, with local minima approximately indicating the start of a new span. The effect of the anomaly is visible by comparison. Different techniques are possible to convert such information into an anomaly location. We estimated the anomaly coordinate by i) finding the time lag of maximum S_i difference, ii) converting it into a coordinate of maximum collision (pulse overlap) by exploiting the time to distance mapping through the walk-off, and iii) removing the estimation bias of the coordinate of the anomaly after 0 km. The results are depicted in Fig. 5.4 (right). The match is very good, with a root mean square error (RMSE) of 4.3 km.

5.2 MONITORING IN PACKET-OPTICAL NETWORKS

As reported in D3.1, the recent evolution of coherent transmission technology has driven the miniaturization of transmitter and receiver components, enabling the reduction from traditional 8RU-size modules to small pluggable form factors such as QSFP-DD (e.g., 400ZR(+) module). In addition to space and power savings, small pluggable form factors will also enable installing coherent modules on off-the-shelf cost-effective packet switches that are designed for data center operations. Such switching platforms already make available impressive throughput performance as well as new programmable functionalities, leveraging on the P4 technology. In D3.1, we showed an innovative P4-based solution specifically designed for packet-optical nodes equipped with coherent pluggable modules and supporting P4 packet switching programmability. The combination of such technologies is particularly attractive since it may lead to both CAPEX and OPEX savings and may enable the removal of standalone transponders (reducing latency while avoiding O/E/O conversions). In D3.1 we presented an innovative monitoring solution exploiting P4 in-network processing to accelerate the exchange and processing of optical telemetry parameters. Such a preliminary solution was applied to a point-to-point configuration.

In this deliverable, we report on a significant enhancement enabling the support of mesh topologies. In particular, a novel framework for in-network P4 processing of distributed multi-layer telemetry data is presented, enabling effective soft failure detection and recovery strategies enforced in just a few microseconds.

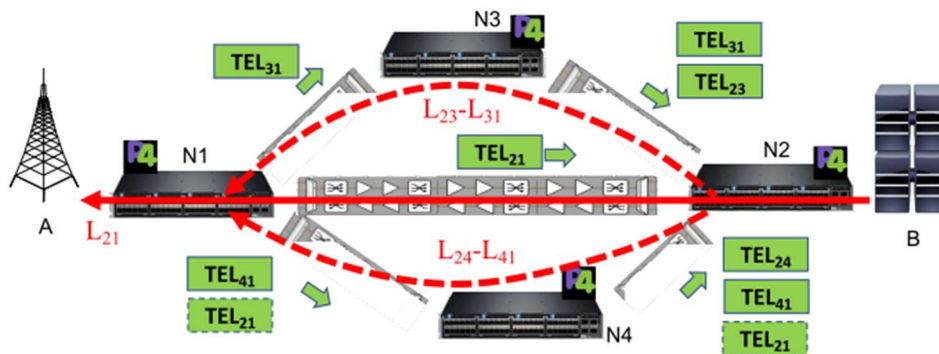


Figure 5-5: reference network scenario

Figure 5-5 shows a network of four p4-enabled packet-optical nodes interconnected through optical line systems. The connectivity between N1 and N2 is served by two unidirectional lightpaths, i.e., L12 and L21. Alternative routes between N1 and N2 are also available, passing through N3 or N4. Each node knows about the QoT of the lightpaths terminated at its coherent receivers (e.g., received OSNR, pre-FEC BER, RX power). In addition, each node has access to the packet level QoS parameters (e.g., in/out packet/bit rates, queue occupation). For example, N2 monitors QoT and QoS of the optical connections originated at N1, N3 and N4, e.g., N2 can immediately detect a (soft) failure affecting L12.

On the one hand, with traditional SDN-based mechanisms, N2 has no direct knowledge of the QoT status of the lightpath in the reverse direction (L21). Upon a soft failure occurrence on L21 (e.g., amplifier malfunctioning, aging), N2 must be rapidly notified by N1. There are effective mechanisms for hard failures, e.g., routing protocol notifications and Bidirectional Forwarding Detection (BFD). On the other hand, since soft failures imply higher pre-FEC BER with sporadic

post-FEC problems, these mechanisms do not operate appropriately since they are based only on up/down status information. Alternative notification methods through a centralized SDN system might not be scalable and sufficiently fast to avoid data losses. Furthermore, even if N2 correctly detects the soft failure, it has no reliable means to quickly identify alternative directions with good end-to-end QoT and QoS. Indeed, N2 has no visibility on the performance of non-directly connected links (i.e., N3-N1 and N4-N1), which, in turn, might also suffer from soft failures and/or might not have sufficient available bandwidth. Also, in this case, leveraging on SDN intervention might not provide timely mitigation. This work introduces a framework that relies on the direct, in-network exchange of Multi-Layer Network Telemetry (MLNT) reports among packet-optical nodes to address these shortcomings. MLNT reports provide detailed real-time performance (i.e., QoT and QoS) of those links that are of interest for a specific node. For example, by retrieving telemetry data from N1, N3, and N4, N2 learns about the status of the outgoing directions on the links that are (in this case) up 1-hop away. N2 can then decide on the most suitable end-to-end B-A connection (i.e., direct L21 as well as either lightpaths L23-L31 or L24-L41 crossing N3 and N4, respectively). The MLNT reports are processed in-network by the P4 ASIC, operating at wire speed. Thanks to its stateful capabilities, P4 operations can then be performed on the retrieved MLNT data. In the proposed framework, the SDN Controller pre-computes the alternative route(s) to be enforced upon a QoT threshold violation for each active lightpath in the network. This is done by considering the actual QoT and QoS performance of each alternative route to make sure their QoT threshold is met, and QoS is appropriate. Then, the SDN Controller compiles the decisions in the form of custom P4 rules to be deployed at the P4 nodes. In the end, the algorithm enforces (e.g., through P4Runtime or Thrift) the flow rules and thresholds to be considered for real-time operations.

The following algorithm illustrates the details of the P4 rules deployed by the SDN Controller at N2 to recover from a potential soft failure on L21. Let Q and T be the set of current QoT measurements and thresholds for each lightpath, respectively, and B be the residual (free) bit rate at each lightpath. First, the script checks if L21 is above its QoT threshold, in which case no action is necessary. Otherwise, the script selects the node (N3 or N4) to be used to re-route the traffic. This is done by first checking if all links of a potential alternative path meet the QoT threshold

and then selecting the alternative route with the highest residual bit rate. This way, when the QoT threshold is exceeded, the P4 ASIC can immediately steer the traffic toward the pre-defined alternative route. The proposed distributed telemetry framework provides detection of failures, including soft ones, and evaluates the performance of suitable end-to-end alternative routes in real time.

```

if  $Q_{L_{21}} \geq T_{L_{21}}$  then
  do_nothing()
else if  $Q_{L_{23}} \geq T_{L_{23}} \wedge Q_{L_{31}} \geq T_{L_{31}} \wedge \max(B_{L_{23}}, B_{L_{31}}) \geq \max(B_{L_{24}}, B_{L_{41}})$  then
  use_route(L23, L31)
else if  $Q_{L_{24}} \geq T_{L_{24}} \wedge Q_{L_{41}} \geq T_{L_{41}} \wedge \max(B_{L_{24}}, B_{L_{41}}) > \max(B_{L_{23}}, B_{L_{31}})$  then
  use_route(L24, L41)
end if

```

Algorithm 5-1

The proposed solution was implemented in a network testbed reproducing Figure 5-5. N2 is a

P4 Tofino switch. N1, N3, and N4 are Mellanox/Nvidia switches equipped with Spectrum1/2 P4 ASIC, SONiC Operating system, and 100G optical pluggable modules. A soft failure is introduced by forcing in-line attenuation. In N1, an application running in SONiC reads the QoT (i.e., RX power) and QoS (e.g., actual bit rates) values of L21 from the Redis database and relies on a thrift connection to write those values within dedicated flow rules. MLNT packets, generated from clones of specific management flows, match those flow rules, and their content is updated accordingly. That is, MLNT packets are filled in using in-network operations that are efficiently handled at wire speed.

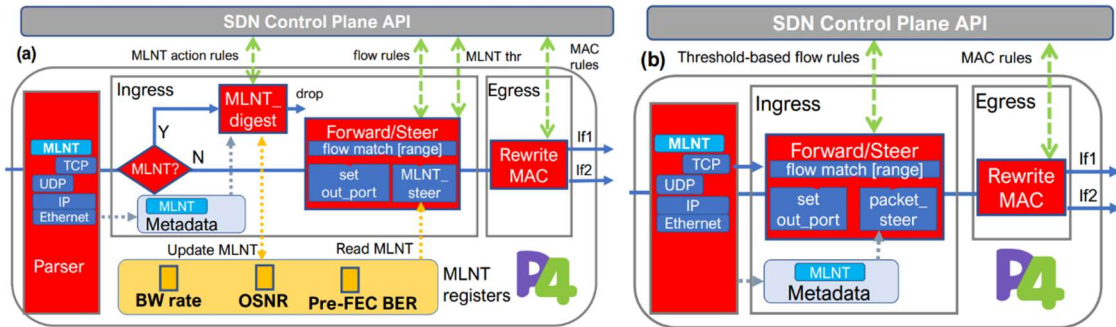


Figure 5-6 P4 design of (a) out-of-band and (b) in-band MLNT-based steering pipelines.

Figure 5-6 shows the two considered P4 implementations. MLNT headers may be sent periodically (out-of-band, O-MLNT) or continuously inside each traffic packet (in-band, I-MLNT). In the O-MLNT case (Figure 5-6a), MLNT messages are processed separately, and the embedded QoT/QoS metrics are stored in dedicated P4 registers, while data traffic is steered based on the current register values (i.e., MLNT steer action). In the I-MLNT case (Figure 5-6b), the MLNT headers are embedded in each packet and matched as metadata against a steering flow table, performing instant forwarding relying on range-based matching (i.e., packet steer action) without requiring any P4 register. When N2 receives the MLNT data, it stores the retrieved values in specifically configured P4 registers (O-MLNT) or processes it in a per-packet fashion (I-MLNT). When pre-defined thresholds are exceeded, L21 traffic flows are rerouted according to pre-installed rules (i.e., either on L23-L31 or L24-L41). Results show that the time from which a MLNT packet triggering the rerouting enters N2 and the time at which the first data packet is forwarded along an alternative direction (e.g., L23-L31) is only around 2 μ s in both I-MLNT and O-MLNT deployments. The MLNT report format is derived from standard INT reports. Each MLNT packet occupies between 60 and 100 bytes. The overall bandwidth consumed by MLNT packets depends on the generation rate. For example, 0.08 Mb/s is obtained in the case of a MLNT packet every 10ms. Even higher rates (e.g., 1 pck/ms) would still occupy less than 0.001% of a 100 Gb/s connection. In these measurements, we limited the forwarding of MLNT data to 1-hop distances. Futures studies may investigate the impact and benefit of encompassing additional/different nodes. Given the processing of data at the HW level, no performance issues are experienced, even at higher rates. This work was published at OFC 2023 Conference [Cug23].

6 TABLE OF PROTOTYPES DEVELOPMENT STATUS AND DELIVERY

Prototypes	Development Status	Software Control Parameters	Software Control Mode	Roadmap to Complete	Delivery Time
MB S-BVT (PtMP transceiver)	Optimization of the S-band contribution/slice	Laser central wavelength (TLS); Laser output power and DAC channels (enable/disable)	SDN OpenConfig agent	1) Performance evaluation and assessment of the optimized MB S-BVT (C+S). 2) Integration with the augment version of the SDN OpenConfig agent.	April 2023
(Semi-) Filterless Node Prototype	Completed	Input and Output port routing.	Matlab-based Instrument Control	N/A	N/A
2-degree C ROADM	Prototype based on discrete component is ready	Explicit/operational mode: drop channels (C-band, add channels (C-bands), drop and continue channels (C-bands), channel power (C-bands)	Config by FPGA	Completed	First of Oct, 2023
2-degree O,C,L ROADM	On going , prototype based on discrete component	Explicit/operational mode: drop channels (O-, C-, L- band) add channels (O-, C-, L-bands), drop and continue channels (O-, C-, L- bands), channel	Config by FPGA	1) Performance assessment. 2) Integration with the SDN OpenROADM agent.	First of Feb, 2024

		power (O-, C-, L-bands)			
MCS switch PIC	In fabrication	Explicit/operational mode: Select the path from the access. Not packaged PIC, test will be done in TUE laboratory.	Config by FPGA	PIC expected by end of Nov,2023. Characterization by end of February 2024. System transmission assessment by end of June 2024.	Chip delivery end of Nov, 2023. Characterization by end of February 2024. System transmission assessment by end of June 2024.
C and L band WSS PIC	In fabrication	Explicit/operational mode: Select the channel in C and L-bands. Not packaged PIC, test will be done in TUE laboratory.	Config by FPGA	PIC expected by end of Nov,2023. Characterization by end of February 2024. System transmission assessment by end of June 2024.	Chip delivery end of Nov, 2023. Characterization by end of February 2024. System transmission assessment by end of June 2024
Power Profile Monitoring DSP Software	Completed	Received Coherent Waveform	HHI's Matlab DSP Toolbox	N/A	N/A
MB Offline Transceiver Prototype	Assembled	Yet to be decided	Matlab-based Instrument Control	Characterization and Testing	Jan/2024

Impairment validation tool	First version completed	Transmitter, receiver and link parameters		Second version under development with improved optimization options	December 2023
7-node mesh network	Completed	Transmitter, receiver, Path, ...	SDN OpenConfig agent	N/A	Feb 2023
Packet-optical white box with SONiC Operating System, OpenZR(+) transceivers	Enhanced SONiC OS support to coherent pluggable transceivers	Transceiver parameters (frequency, power, application code) packet forwarding rules	OpenConfig SDN Agent with telemetry support	Pre-final. Application code adaptation to be finalized and verified	Jan 2024
P4 switch	Software switch (P4 ASIC not yet available on white box supporting coherent pluggable modules)	Few rules, optical transmission parameters embedded within in-band telemetry	P4runtime	Final	Oct 2023
Multiband Amplifier	Verification of the feedforward control for operation of a C-band and L-band system			N/A	January 2024
S-band	Going integration with C+L band amplifier	N/A	N/A	N/A	March 2024

7 CONCLUSIONS

This report provides an overview of WP3's activities during the second year of the project, focusing on the utilization of the D3.1 reference architecture. It centers on three reference time frame scenarios: short-term (approximately 3 years from the present), mid-term (around 6 years), and long-term (about 9 years). Each scenario includes estimated traffic demands, forming the foundation for the introduction of new technologies and architectures in various network segments over time.

In metropolitan networks, the report suggests deploying C+L band systems or SDM in the short-term, while the C-band, currently deployed, is expected to meet mid-term requirements. In the long-term, C+L band systems, full multi-band systems, or SDM may be needed in the core and backbone networks, emphasizing the importance of multi-band technology and SDM for evolving network demands.

The development of MB S-BVT is progressing, with optimization efforts focusing on S-band amplification, programmable S-band filters, and improved tunable laser sources. These refinements aim to enhance multi-band transmission systems, with an optimized prototype expected by M30.

Development is underway for a flexible, high-capacity multi-frequency optical switching integrated solution for B5G networks, featuring a customizable MB-OADM. Its practical deployment in metropolitan access networks for aggregating Xhaul traffic is discussed, along with the design of optical integrated chips.

Progress in developing multi-band optical amplifiers is highlighted, emphasizing the fine-tuning of amplifier gain and tilt for consistent OSNR across channels and the role of Raman amplification, especially in the S-band.

In the physical layer design, a filter-less solution is proposed for metropolitan aggregation networks. It covers various network topologies and hardware optimizations, delving into the design and functionality of filter-less add/drop nodes and their role in achieving multi-band scalability.

The architecture of optical access networks necessitates the integration of X-Haul options, accomplished through the adoption of the access planning tool introduced in D4.2. Additionally, the report discusses the convergence of wired and wireless technologies through LiFi, showcasing its seamless integration with broader network infrastructure.

Lastly, the document explores various monitoring techniques to enhance network surveillance and provide real-time performance data for effective anomaly detection and network management improvement. It includes methods such as longitudinal power profile monitoring using coherent receivers, fiber loss anomaly localization through cross-phase modulation, and the application of P4 technology to optimize optical network performance.

8 REFERENCES

- [Cug23] F. Cugini, C. Natalino, D. Scano, F. Paolucci and P. Monti, "P4-based Telemetry Processing for Fast Soft Failure Recovery in Packet-Optical Networks," 2023 Optical Fiber Communications Conference and Exhibition (OFC), San Diego, CA, USA, 2023, pp. 1-3, doi: 10.1364/OFC.2023.M1G.2
- [Hyu20] Hyun-Do Jung, et. al., "Polymer-based optical switch for future metro-area networks," OSA Advanced Photonics Congress (APC), paper PsTh3F.2, Optica Publishing Group (2020).
- [Kir83] S. Kirkpatrick, C.D. Gelatt Jr and M.P. Vecchi, "Optimization by simulated annealing". Science, vol. 220, no. 4598, pp. 671-680, May 13, 1983.
- [Mun17] R. Muñoz, L. Nadal, R. Casellas, M. S. Moreolo, R. Vilalta, J. M. Fabrega, R. Martínez, A. Mayoral, and F. J. Vílchez, "The ADRENALINE testbed: An SDN/NFV packet/optical transport network and edge/core cloud platform for end-to-end 5G and IoT services," (2017), pp. 1–5.
- [Nad22] L. Nadal, M. S. Moreolo, J. M. Fàbrega and F. J. Vílchez, "SDN-Enabled Multi-Band S-BVT Within Disaggregated Optical Networks," in Journal of Lightwave Technology, vol. 40, no. 11, pp. 3479-3485, 1 June1, 2022, doi: 10.1109/JLT.2022.3158388.
- [Nad23] L. Nadal, R. Casellas, J. M. Fàbrega, F. J. Vílchez and M. Svaluto Moreolo, "Capacity Scaling in Metro-Regional Aggregation Networks: the Multiband S-BVT", accepted in JOCN, Special Issue on Advances in Multi-Band Optical Networks, June 2023.
- [JOCNPedro] João Pedro and Nelson Costa, "Hybrid amplifier placement in mesh DWDM networks using integer linear programming models," J. Opt. Commun. Netw. 15, E29-E39 (2023)
- [RUI23]https://www.researchgate.net/publication/372473374_Network_Traffic_Analysis_under_Emerging_Beyond-5G_Scenarios_for_Multi-Band_Optical_Technology_Adoption M. Ruiz, J.A. Hernandez Gutierrez, M. Quagliotti, E. Hugues-Salas "Network Traffic Analysis under Emerging Beyond-5G Scenarios for Multi-Band Optical Technology Adoption", Journal of Optical Communications and Networking, July 2023, DOI:10.1364/JOCN.492128
- [Uzu21a] D. Uzunidis, E. Kosmatos, C. Matrakidis, A. Stavdas and A. Lord, "Strategies for Upgrading an Operator's Backbone Network Beyond the C-Band: Towards Multi-Band Optical Networks," in IEEE Photonics Journal, vol. 13, no. 2, pp. 1-18, April 2021.
- [Uzu21b] D. Uzunidis, C. Matrakidis, E. Kosmatos, A. Stavdas, P. Petropoulos, A. Lord, "Connectivity Challenges in E, S, C and L Optical Multi-Band Systems", in European Conference of Optical Communications, ECOC' 21, 2021.
- [XIA23] S. Xia et al. "Performance Assessment of Multiband OADM in Metro-Access Network for Converged Xhaul Traffic", ECOC 2023, Tu.A.5.5.
- [Tan19] T. Tanimura et al., "Experimental demonstration of a coherent receiver that visualizes longitudinal signal power profile over multiple spans out of its incoming signal," presented at the European Conference on Optical Communications (ECOC), 2019, pp. 1-4.
- [Tan20] T. Tanimura et al., "Fiber-Longitudinal Anomaly Position Identification Over Multi-Span Transmission Link Out of Receiver-end Signals," J. Lightwave Technol., vol. 38, no. 9, 2020, pp. 2726–2733.

[Sas21] T. Sasai et al., "Revealing Raman-amplified Power Profile and Raman Gain Spectra with Digital Backpropagation," presented at the Optical Fiber Communications Conference and Exhibition (OFC), 2021, pp. 1-3.

[MAY23] May, Alix, et al. "Longitudinal Power Monitoring over a deployed 10,000-km Link for Submarine Systems." 2023 Optical Fiber Communications Conference and Exhibition (OFC). IEEE, 2023.

[Hui22] Hui, Rongqing, Charles Laperle, and Maurice O'Sullivan. "Measurement of Total and Longitudinal Nonlinear Phase Shift as Well as Longitudinal Dispersion for a Fiber-Optic Link Using a Digital Coherent Transceiver." *Journal of Lightwave Technology* 40.21 (2022): 7020-7029.

[Dar16] Dar, Ronen, et al. "Pulse collision picture of inter-channel nonlinear interference in fiber-optic communications." *Journal of Lightwave Technology* 34.2 (2016): 593-607.